

E-Mobility Charging

ECE Capstone II Final Report

Fall 2023



Advisor

Professor Masoud Salehi

Capstone Group M2

Ali Hussein
Alex Zabib
Ezekiel Gunnison
Valentina Ribeiro
Grady Kirsch
Michael Montanaro

Table of Contents

Abstract.....	2
1 Introduction.....	4
1.1 Background Information.....	4
1.2 Problem Statement.....	4
1.3 Solution Overview.....	5
2 Project Breakdown.....	6
2.1 Mechanical Breakdown.....	6
2.2 Charge Controller.....	8
2.2.1 LT8490 Configuration.....	10
2.2.2 Input Voltage Sensing.....	16
2.2.3 PCB Design.....	16
2.2.4 Testing.....	17
2.2.5 Full Charge Controller Schematic.....	18
2.3 2-Stage Inverter.....	18
2.3.1 Boost Converter.....	20
2.3.2 Inverter Stage.....	21
2.3.3 PCB Design.....	23
2.3.4 Testing.....	26
2.3.5 Full Inverter Schematic.....	27
2.4 Software Ecosystem.....	27
2.4.1 App Development.....	27
2.4.2 Microcontroller Software Development.....	28
2.4.3 Message Protocol.....	29
2.4.4 Development Process.....	29
2.5 Scaled System Simulation.....	30
2.5.1 Overview.....	31
2.5.2 Solar Panels and Charge Controller.....	33
2.5.3 Battery and DC-DC Converter.....	35
2.5.4 Inverter and Filter.....	36
2.5.5 Grid and Load.....	37
2.6 Prototype Efficiency.....	38
3 Project Planning.....	39
3.1 Timeline.....	39
3.2 Task Breakdown.....	40
3.3 Resource Allocation.....	41
3.4 Communication.....	43

4 Results.....	43
4.1 Mechanical System.....	43
4.2 Charge Controller.....	44
4.3 2-Stage Inverter.....	45
4.4 Software Ecosystem.....	45
4.5 Simulation.....	46
5 Conclusion.....	51
5.1 Improvements.....	51
5.1.1 Mechanical System.....	51
5.1.2 Charge Controller.....	52
5.1.3 2-Stage Inverter.....	52
5.1.4 Software Ecosystem.....	52
5.1.5 Simulation.....	53
5.2 Scaling and Next Steps.....	53
5.3 Closing Remarks.....	54
6 Compliance.....	54
7 Acknowledgment.....	54
References.....	55

Abstract

Our team designed a solar powered charging station for e-mobility that provides accessible charging to university students whose institutions place restrictions on indoor charging. The rise and popularity of modes of e-mobility like electric bikes and scooters has led to cases of battery-related fires on campuses; pressuring administrations for issuing bans on e-mobility. This design proposes an outdoors charging station, employing a charge controller and inverter, whose power delivery is regulated by an app.

The system contains a 5x2 solar photovoltaic array arrangement using a total of 10 panels that is pole-mounted at a height of 7 feet atop a concrete-anchored base. The electronic components are housed in a NEMA 3R-rated enclosure and the system is grounded with an external earthing design utilizing 3 parallel steel electrodes. The enclosure contains circuit subsystems consisting of a charge controller and inverter. The charge controller connects the solar panel to the internal battery of the system. The purpose of the converter is to regulate the voltage produced by the solar panel to match the specifications of the internal battery, while employing a maximum power point tracking (MPPT) algorithm to maximize the power generated by the panels. The controller responsible for this regulation is capable of temperature measurement of the internal battery and input/output voltage sensing. The inverter is designed to draw from the battery and output 120VAC; providing up to 300W to the e-mobility. It employs an ESP32 utilizing a Sinusoidal Pulse Width Modulation (SPWM) to generate the output sine wave, as well as facilitate seamless communication between the app and the physical charging system. An MQTT broker setup using Eclipse Mosquitto is employed, ensuring efficient real-time data exchange. Hosted on an EC2 instance, the MQTT broker establishes a scalable and reliable connection, laying the foundation for

potential future integrations in smart charging solutions. This innovative approach enhances the charging system's functionality, contributing to a more efficient and controlled energy transfer process. This control scheme underscores a streamlined approach to mobile app development, emphasizing security, user experience, and advanced communication protocols, complemented by a novel technique of SPWM for optimal charging system performance.

To model the scalability of the microgrid, a simulation was performed using Simulink and Simscape electrical toolbox. The model shows the main subsystems, simulates Boston irradiance data for the panels, and includes an additional interconnection with the national grid. The system aims to model a scaled up version of our design, capable of a larger load that supports up to ten E-bikes, sourcing a solar farm array and large battery storage, and employing a bidirectional, grid-connected inverter designed that complies with national grid standards regarding voltage and frequency thresholds.

Testing and validation was performed on the charge controller and inverter. The charger controller had its MPPT abilities tested on a solar panel. The inverter was tested for its ability to generate the 120VAC for a range of voltages that simulate the charge profile of the battery. The powering of the load was initiated by the app to emulate a user charging their e-mobility at a station, as the goal of the design to provide a reliable and accessible charging method for students that overcomes indoor charging restrictions.

1 Introduction

1.1 Background Information

E-mobility is defined as an electric-propulsion based transportation in the form of a lightweight, low-speed, single-person vehicle. These include electric scooters, bikes, skateboards, etc. The emergence of e-mobility was a product of docked, shared mobility programs, in this case bike sharing programs, that were implemented in Asia in the early 2010s. China was the first to adopt this in an effort to address mobility issues and excess vehicle emissions. Dock stations allowed consumers to rent from kiosks and return the bike to any suitable station. These were located near public transportation to further encourage people to use the train and bus systems. Ofo was the first successful mobility shared company, deploying more than 10 million bikes worldwide. Later startups began branching to dockless mobility, allowing users to unlock and pay for rentals from the convenience of an app. Free from the restriction of dock stations, users began to travel further distances, which prompted the development of e-mobility to accommodate as they provide anywhere from 10 to 40 miles on a full charge. [1] [2]

E-mobility, predominantly e-scooters, quickly became a preferred shared mobility program in the US; achieving 86 million trips in 2019 alone. Bird and Lime have remained at the top of the e-mobility market since 2017, both of whom are dockless programs. Other rideshare companies began establishing themselves on university campuses and company facilities, offering accessible and sustainable transportation for students within the surrounding area. This boom of shared mobility bolstered the direct to consumer (D2C) e-mobility market as many consumers preferred ownership over rentals. As of 2022, over 5 million units have already been sold in the US alone, with 17 million expected by 2030. Incentives and rebates prompted growth of not only e-mobility, but their associated charging stations. Ride share programs would either establish their own charging infrastructure or contract with companies that only develop charging solutions. Bikeep and Knot are two of the largest e-scooter charging companies, offering wired and wireless charging solutions while facilitating the growth of e-mobility across the country and abroad. [3] [4]

1.2 Problem Statement

Among ridesharers and D2C owners, there are 3 issues that prevent e-mobility growth. The first is in regard to safety. The most common component of failure in e-mobility is the battery, particularly lithium ion batteries which are the most popular battery type. Mechanical stress, overcharging, use of low quality components, rapid discharging, and over-temperature are but a small list of causes of battery thermal runaway fires. This has led institutions and universities alike to ban charging inside buildings due to safety concerns. [1]

Another issue is the cluttering of e-mobility in public spaces. Dockless, rideshare e-mobility are major contributors as consumers leave their mobility in areas that can obstruct pedestrians walking, vehicles parking, and other e-mobility users. In addition, e-mobility owners often leave their devices

laying haphazardly or lock it onto various areas. Without designated parking, disruption of mobility in urban cities will continue to be a criticism of e-mobility. [5]

Lastly, there is lack of accessibility. Urban infrastructure for ridesharing typically doesn't incentivize consumers to use e-mobility. Presentation of e-mobility sites is poor, with devices often scattered around, vandalized, or damaged from thieves due to a lack of security. Furthermore, charging infrastructure is often placed in inconspicuous areas where users would not notice it. This deters one of the goals of cities where e-mobility be located near bus and train stations to encourage intermodal transportation, prompting users to rely on solely public transport or walk to their destination. E-mobility owners typically don't have access to public charging, not even outlet charging in public areas due to bans regarding battery safety. Majority of charging options are tied to rideshare programs, many of whom don't allow non-rideshare devices to be charged. The few that do charge per kWh in addition to a service fee, making users, particularly low income users, feel inconvenienced to charge their device. [5] [6]

1.3 Solution Overview

To address concerns regarding safety, clustering prevention, accessibility, and limited charging, our team aims to develop a cost effective, renewable charging solution for e-mobility owners and rideshare users while meeting safety and reliability standards that comply with building requirements. The solution will be targeted to Northeastern students, but can be scaled to urban and commercial applications. The charging solution will be solar powered and completely off-grid, allowing it to be strategically placed near public transport and other convenient sites to encourage its users and prevent dockless devices from cluttering on the streets. In addition, the AC output can accommodate any wired e-mobility device, thus opening public charging to e-mobility users. Most of all, the experience will be simplified via a user notification app; alerting the user of their charge time, charge location, and other logistical information. Though the system will be isolated from the grid, an on-grid system that can support additional charging devices can be simulated to showcase the above features on a larger scale and meet higher load demands.

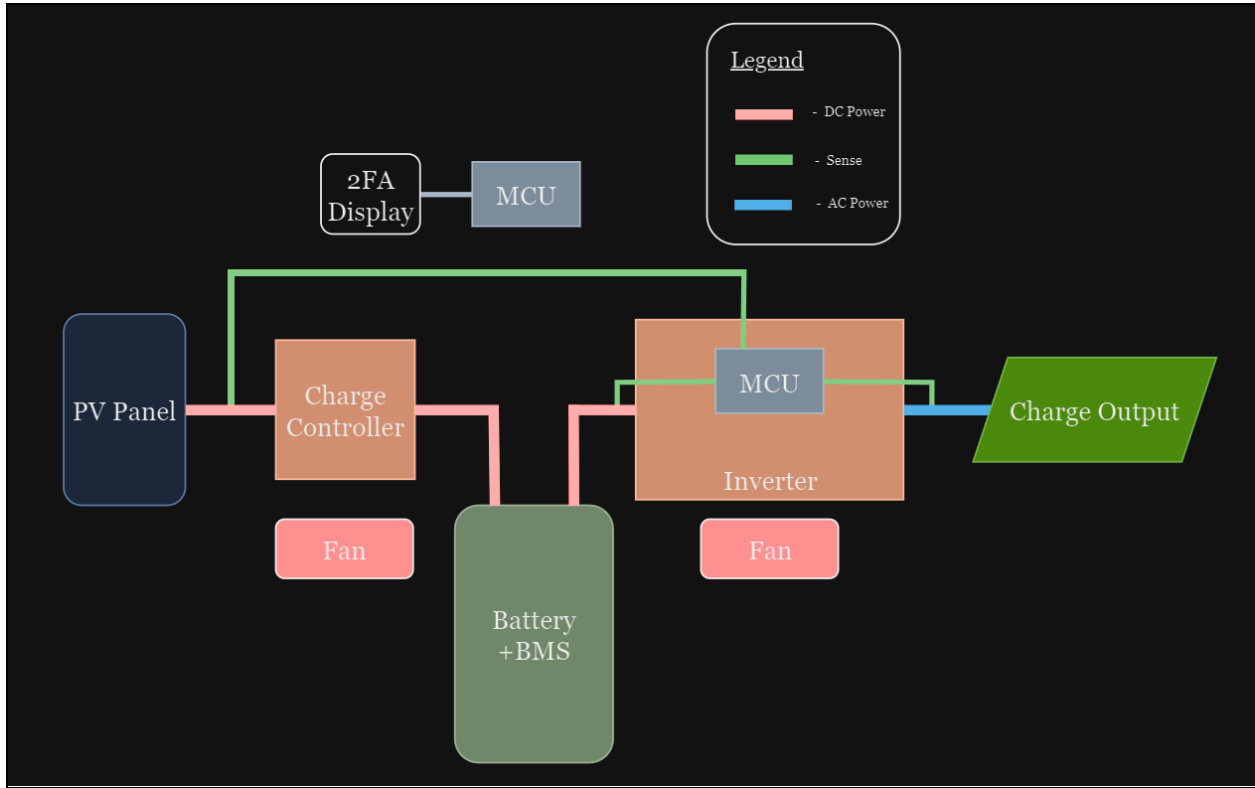


Figure 1.3.1: Block Diagram of the Prototype

2 Design and Implementation

This section takes an in-depth look at the finalized prototype for each subsystem. We observe the purpose and details behind each one, ascertain why said approaches were taken, how they were implemented, and overlook each subsystems testing procedures. The selection and construction of mechanical components are described in detail, including the solar panel mounting, enclosure selection, and grounding considerations. The design and functionality, as well as component selection and PCB layout for the charge controller and inverter are noted off. The features and applications of the app services' communication and MQTT broker setup are detailed. Lastly, the tools and testing of the large scale simulation are presented.

2.1 Mechanical Breakdown

This installation leverages a lateral pole PV mount with a 5x2 solar photovoltaic array arrangement at a height of 7 feet, situated atop a concrete-anchored base. Directly below is a weatherproof enclosure to provide sustainable charging outdoors to one e-mobility load. The mechanical structure is critical for durability, safety, security, ergonomic maintenance access, and overall functionality. This system is designed to prevent damage, theft, and fall hazards.

Mounting System

This system utilizes a solar array affixed to a mounting plate to ensure stability. It features a side pole mounting bracket secured to a 7ft Schedule 40 PVC pole for structural support. The PVC pole offers economical support compared to pricier metal alternatives. The design incorporates a 5/8 in. x 2 ft. x 4 ft. oriented strand board (OSB), prioritizing its inherent strength, durability, and resistance to deflection, delamination, and warping. A flame-retardant coating fortifies the OSB board for heightened fire protection. This economical choice stands in contrast to the commonly applied galvanized steel or aluminum in side-pole solar mounting. Additionally, a lightweight 5 lb mounting bracket with angular adjustments facilitates seasonal solar tracking for optimal sunlight capture. The mount orientation is angled at 42° to maximize solar energy generation at this latitude. The mounting bracket is robust, ensuring its stability in severe wind conditions through high-strength bolts. The mount also employs corrosion-resistant aluminum alloys and stainless steel fasteners to withstand the elements over time.

At the base of the system, a concrete bucket foundation provides weight and anchoring for the entire structure. Instead of using a ground screw for the base, we opted for a bucket of Quickcrete due to its cost-effectiveness, rapid setting, and portability to ensure easy transport for the presentation. In addition to the pole, the concrete base raises the solar array to an optimal height to avoid tampering.

Electrical Enclosure

In accordance with NEC 314, we selected a lockable, 50x40x20cm NEMA IP66-rated steel enclosure designed to withstand outdoor environments. Its epoxy polyester-coated carbon steel construction protects the charge controller, battery, and inverter. The enclosure features a cable entry gland for wire pulling and a 15A flush-mounted recessed duplex receptacle for seamless integration of the e-mobility power adapter. Additionally, the lockable enclosure deters tampering and provides security from public access. The enclosure allows for proper ventilation and component layout to prevent overheating. Positioned at the rear of the assembly, it prevents interference with the solar panels when opened.

Grounding

The system employs an above-ground earthing setup in accordance with the National Electrical Code (NEC) 250.53 (A.2) for safety and protection. This specifies that a single ground rod should have a maximum resistance to ground of 25Ω . If this resistance is not met, an additional ground rod is required. Mobility constraints drive the grounding design featuring three 2 ft. copper ground rods bonded via galvanized clamps in a horticultural substrate, forgoing a singular, permanent 8 ft. rod. This portable setup pairs seamlessly with the quick-setting concrete bucket anchoring the mechanical structure. An ohm meter was used to test the conductivity of the earthing setup. An initial ohm meter test revealed high resistance in the 10^4 range due to dry and resistive soil conditions. The addition of a salt solution enhances soil conductivity, allowing electrical charges to move more freely and substantially reducing resistance. This adjustment ensures compliance with NEC standards by dramatically increasing ionization and mobility of charge carriers in the substrate. If the resistance to ground is above 25Ω , it could increase the risk of electrical shock since the electrical current might find an easier path to Earth through other means.

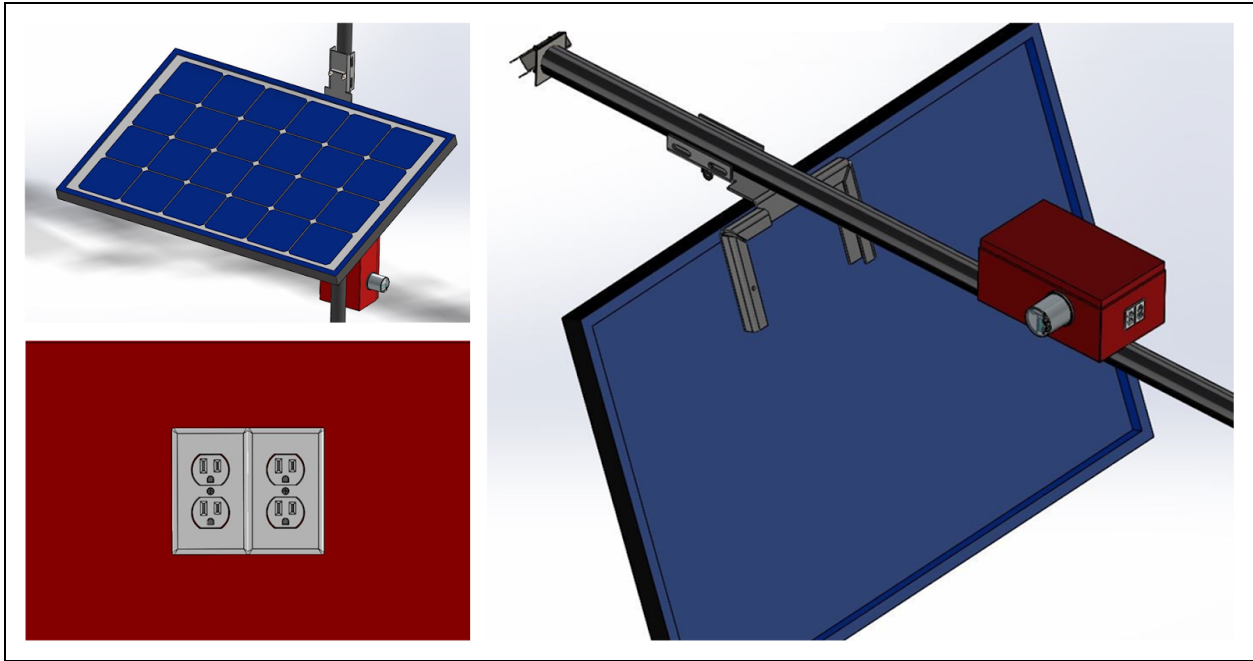


Figure 2.1.1: 3-D Model of Prototype

2.2 Charge Controller

The electrical system of the e-mobility charger is comprised of switching converters. A switching converter can convert electricity from one form to another by utilizing fast power switches (ex: MOSFETs) to regulate the flow of energy in passive components like inductors and capacitors, which are then fed to a load. Stepping up or down an input voltage to meet a required output voltage is the purpose of a DC/DC converter, and if the desired output is an AC voltage, then an inverter is capable of converting DC to AC. The converter architecture in this system consists of 2 converters: a DC/DC converter as the charge controller and inverter to supply power to the e-mobility.

The PV array that will supply power to the system does not produce a constant voltage because of the time of day or weather conditions. To charge the battery however, a constant voltage is required. Otherwise, the battery might not charge or will be destroyed by high voltages. The DC/DC converter is used to regulate the voltage produced by the PV array to prevent any damage to the battery and maximize charging time. As seen in Figure 2.2, the converter will be based around the LT8490 - High voltage, High current Buck-Boost battery charge controller with maximum power point tracking. [7]

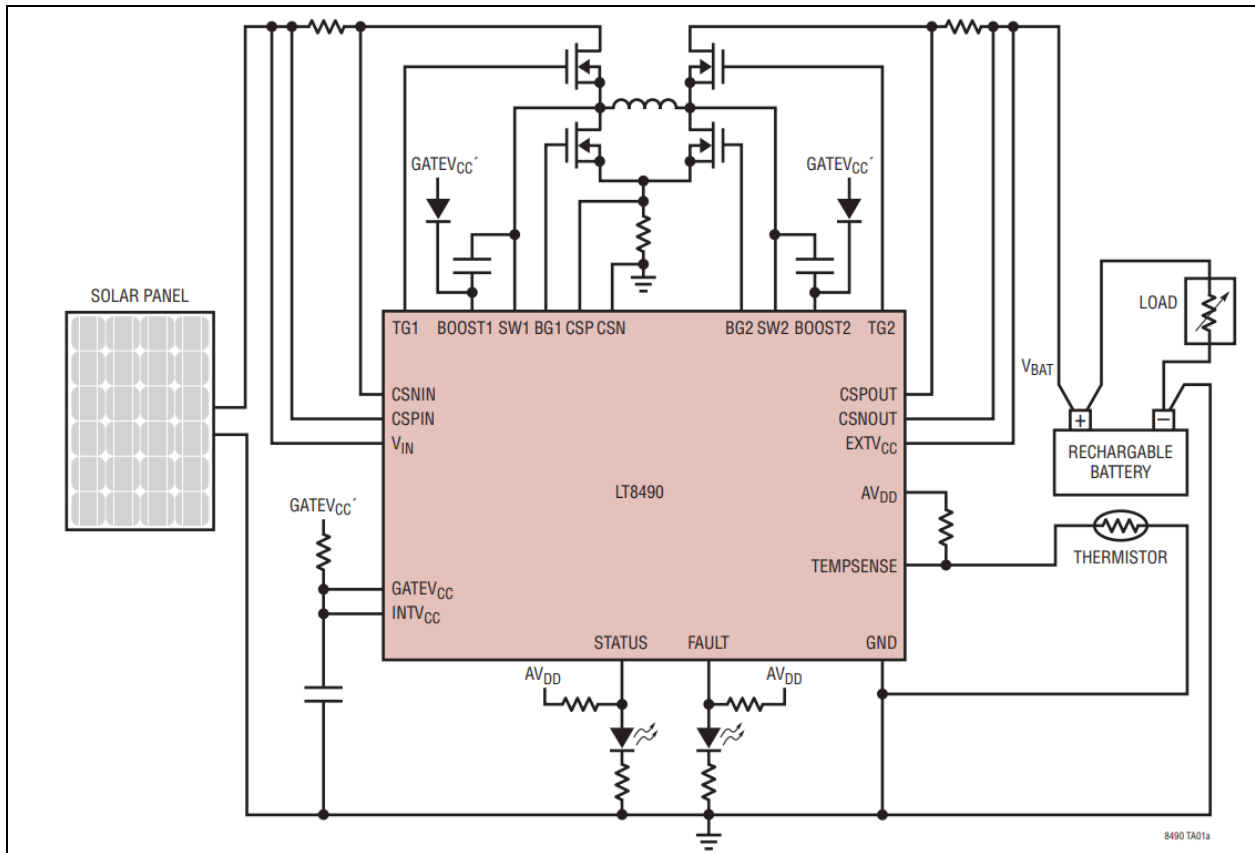


Figure 2.2: Simplified Solar Powered Battery Charger Schematic for LT8490 IC[7]

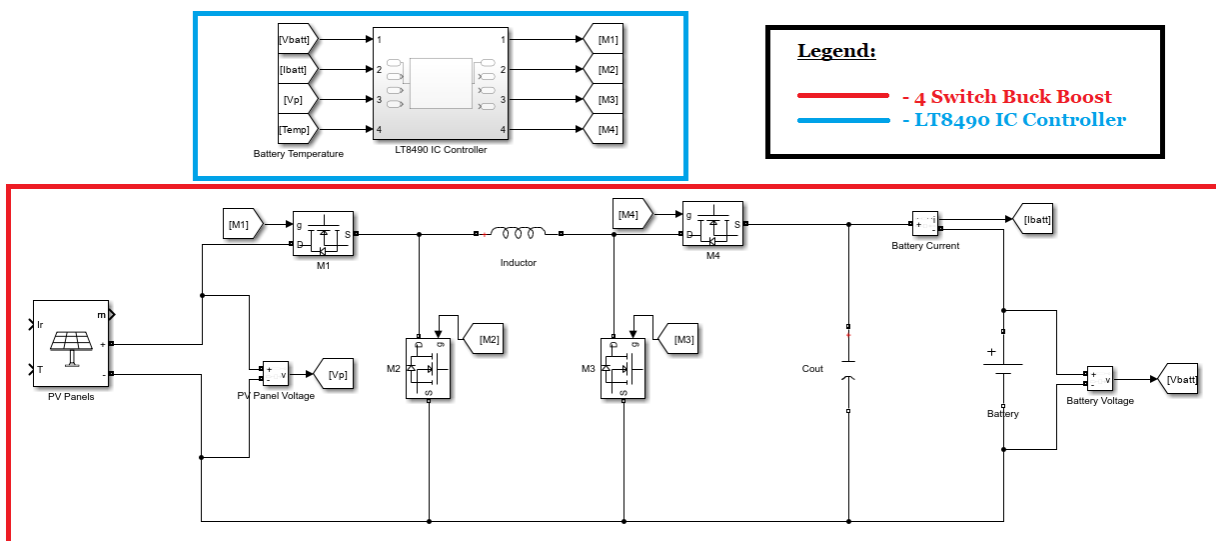


Figure 2.3: Simple Schematic of Charge Controller System

2.2.1 LT8490 Configuration

The LT8490 has a battery charging algorithm that not only maximizes charging time, but also prevents the battery from overcharging or overheating. This algorithm has four charging stages based on the input voltage and current supplied by the PV array, and the charge of the battery. The first charging stage, called trickle charge, occurs when the battery is between 35-70% charged. The battery is charged with a reduced constant current to slowly charge the battery and prevent overcharging. The second charging stage, called constant current, occurs when the battery is between 70-98% charged. The battery is charged with the maximum charge current to ensure that the battery reaches its peak charge. The third charging stage, called constant voltage, applies a constant voltage to the battery to keep it near the 98% charge. The charge current tends to decrease in this stage to prevent overcharging of the battery while trying to maintain its charge.[7] These charging states can be seen in figure 2.2.1. When the battery is below 35%, the LT8490 halts all charging, as it is unsafe to rapidly charge a discharged li-ion battery because when at low voltages the metals inside of the battery can corrode leading to a short-circuit inside of the battery. [7] [8]

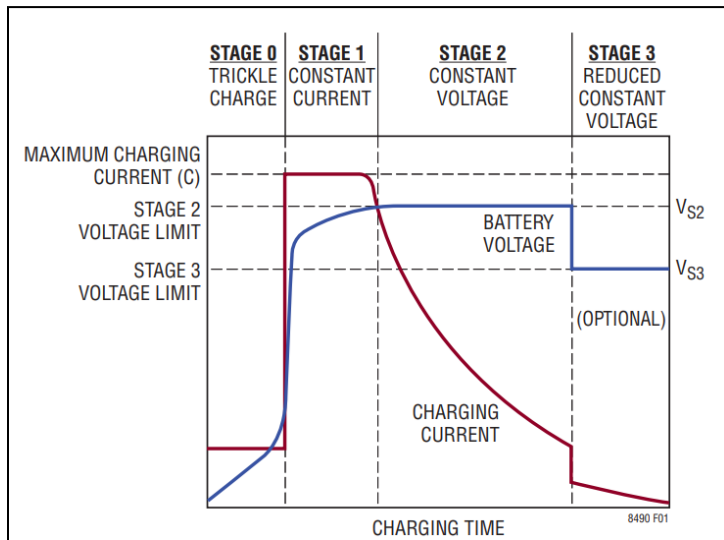


Figure 2.2.1: Constant Current/Constant Voltage Charging Cycle[7]

Stage 3, or float charging, was disabled because lithium-ion batteries don't require float charging. This was done by pulling the CHARGECONFIG1 pin of the LT8490 to 5V. Pulling this pin high also enabled temperature compensated voltage limits, so a thermistor thermally coupled to the battery could monitor its temperature and turn off the system if the temperature of the battery exceeded a certain range. The CHARGECONFIG2 pin was pulled to ground to set the temperature range from 0C to 50C and also disable charge time limits. The LT8490 only supports charge time limits when using a DC power supply. The LT8490 was set to operate in solar panel mode, as the goal is to charge the internal battery by using the solar panels. To set the LT8490 in solar panel mode, the VINR pin was connected to the resistor divider circuit shown in figure 2.2.2.

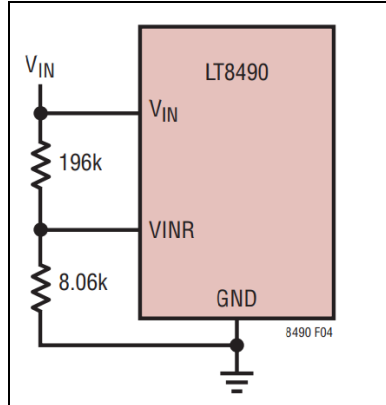


Figure 2.2.2: Solar Panel Enable Circuit[7]

Because of the solar panel configuration used, the maximum input voltage was set to 68V. Based on the maximum voltage, the datasheet provides equations for resistors and capacitors used in the input feedback resistor network as seen in figure 2.2.3.

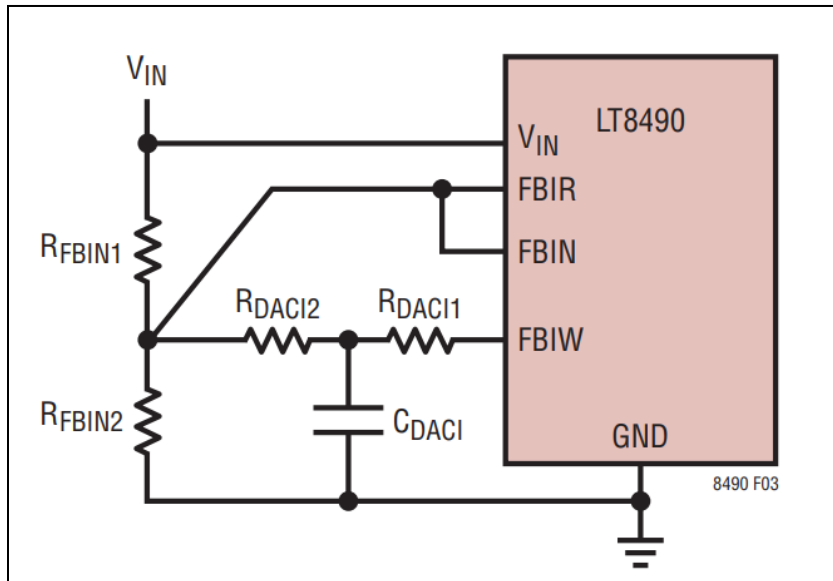


Figure 2.2.3: Input Feedback Resistor Network[7]

The equations used and values for each component can be seen in table 2.2.1.

Component	Equation	Calculated Value	Value used
R_{FBIN1}	$R_{FBIN1} = 100k \cdot \left[\frac{1 + \left(\frac{4.470V}{V_{MAX} - 6V} \right)}{1 + \left(\frac{5.593}{V_{MAX} - 6V} \right)} \right] \Omega$ [7]	98.338kΩ	98.8kΩ

R_{DACI2}	$R_{DACI2} = 2.75 \cdot \left(\frac{R_{FBIN1}}{V_{MAX} - 6V} \right) \Omega$ [7]	4.361kΩ	4.3kΩ
R_{FBIN2}	$R_{FBIN2} = \frac{1}{\left(\frac{1}{100k - R_{FBIN1}} \right) - \left(\frac{1}{R_{DACI2}} \right)} \Omega$ [7]	2.685kΩ	2.7kΩ
R_{DACI1}	$R_{DACI1} = 0.2 \cdot R_{DACI2} \Omega$ [7]	872.2Ω	970Ω
C_{DACI}	$C_{DACI} = \frac{1}{1000 \cdot R_{DACI1}} F$ [7]	1146.5nF	1000nF

Table 2.2.1: Input Feedback Resistor Network Equations and Values

Because the calculated resistor values were such specific values, it was difficult to find those components and if found, were too expensive to use. So, the values were rounded to find components that were cheaper. The datasheet also provides equations to check that your chosen resistors still limit the voltage to your desired value. These equations and checked values can be seen below in table 2.2.2. Vx2 is the maximum desired voltage and Vx1 needs to be as close to 6V as possible.[7]

Equation	Value
$V_{X2} = 1.205 \cdot \left[\frac{R_{FBIN1}}{R_{DACI1} + R_{DACI2}} + \left(\frac{R_{FBIN1}}{R_{FBIN2}} \right) + 1 \right]$ [7]	67.889V
$V_{X1} = V_{X2} - 3.3 \cdot \left(\frac{R_{FBIN1}}{R_{DAC1} + R_{DAC2}} \right)$ [7]	6.0227V

Table 2.2.2: Input Feedback Resistor Network Check Equations and Values

These values are near the desired max voltage and 6V. To set the stage voltage limits for the charging profiles the output feedback resistor network as need in figure 2.2.3 needed to be implemented. The second stage voltage limit was set to 54.6V, which is the typical maximum voltage for a 48V lithium-ion battery.

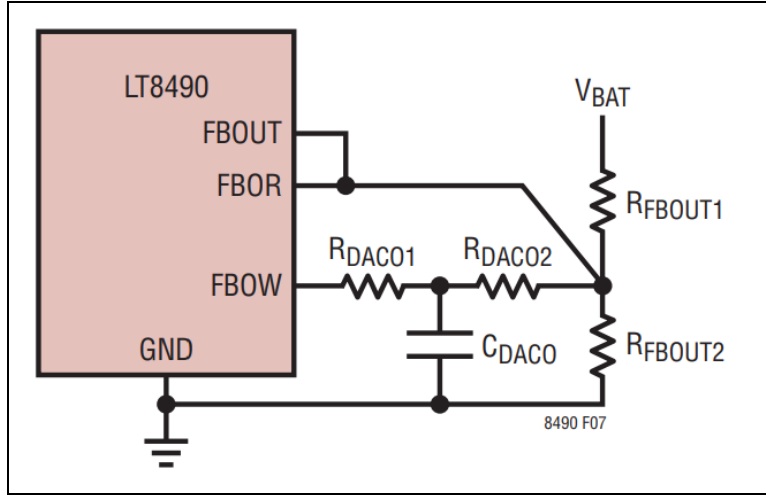


Figure 2.2.4: Output Feedback Resistor Network[7]

The equations used and values for each component can be seen in table 2.2.3 below.

Component	Equation	Calculated Value	Value used
R_{FBOUT1}	$R_{FBOUT1} = R_{FBOUT2} \cdot \left[V_{S2} \cdot \left(\frac{1.241}{1.211} - 0.128 \right) - 1 \right] \Omega$ [7]	1.19MΩ	1.2M
R_{DACO2}	$R_{DACO2} = \frac{R_{FBOUT1} \cdot R_{FBOUT2} \cdot 0.833}{\left(R_{FBOUT2} \cdot V_{S2} \cdot \frac{1.241}{1.211} \right) - R_{FBOUT2} - R_{FBOUT1}} \Omega$ [7]	142.9kΩ	143kΩ
R_{FBOUT2}	R_{FBOUT2} is often chosen between 4.99kΩ and 49.9kΩ. [7]	25kΩ	25kΩ
R_{DACO1}	$R_{DACO1} = 0.2 \cdot R_{DACO2} \Omega$ [7]	28.6kΩ	29kΩ
C_{DACO}	$C_{DACO} = \frac{1}{500 \cdot R_{DACO1}} F$ [7]	68.9nF	100nF

Table 2.2.3: Output Feedback Resistor Network Equations and Values

Similar to the input feedback resistor network, the calculated value for the components were too difficult to find or too expensive. So, the values selected were similar to the calculated values and below in table 2.2.4 are the equations to check if the values selected still produce the desired output voltage. N1 should be close to 1.22 and N2 should be close to 0.805. [7]

Equation	Value
$V_{X3} = \left(\frac{R_{FBOUT1}}{R_{DAC01} + R_{DAC02}} \right) \cdot (X - 1.89)$ where $X = 1.211 \cdot \left[1 + \left(\frac{R_{DAC01} + R_{DAC02}}{R_{FBOUT2}} \right) + \left(\frac{R_{DAC01} + R_{DAC02}}{R_{FBOUT1}} \right) \right]$ [7]	54.601V
$N1 = \frac{X - 1.89}{X - 3.3}$ [7]	1.21975
$N2 = 1 - \frac{1.89}{X}$ [7]	0.80548

Table 2.2.4: Output Feedback Resistor Network Check Equations and Values

After setting the limits on the input and output voltage, the input and output current were limited using the circuit shown in figures 2.2.5 and 2.2.6, respectively.

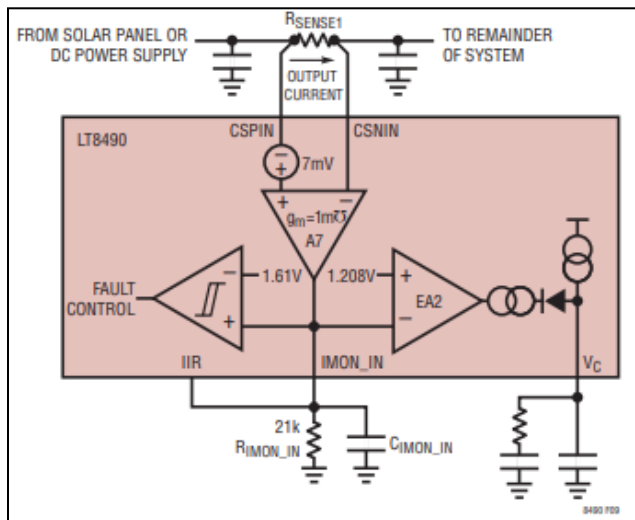


Figure 2.2.5: Input Current Regulation Loop[7]

The equations used and values for each component can be seen in table 2.2.5 below. The value for $I_{in(max)}$ was set to 10A.

Equation	Value
$R_{SENSE1} = \frac{1000 \cdot \left(\frac{1.208V}{21k\Omega} - 7\mu A \right)}{I_{IN(MAX)}} = \frac{0.0505}{I_{IN(MAX)}} \Omega$ [7]	5mΩ

Table 2.2.5: Input Current Regulation Loop Equations and Values

The resistor chosen for Rsense1 was also rated to handle .5W. Below in figure 2.2.6 is the output current regulation loop.

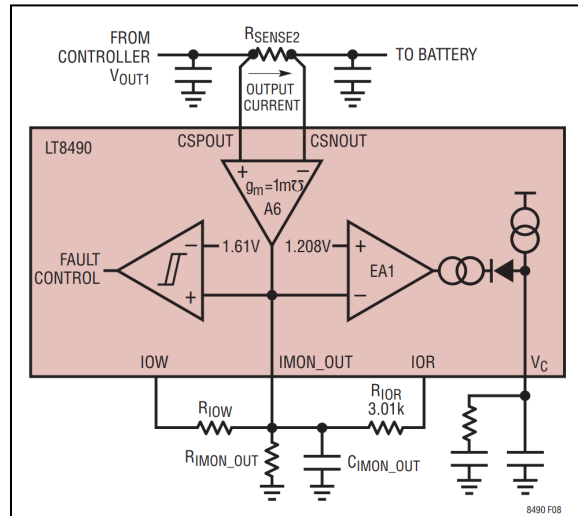


Figure 2.2.6: Output Current Regulation Loop[7]

The equations used and values for each component can be seen in table 2.2.5 below. The output current was set to max at 25A. $I_{out(maxs0)}$ is the current limit for stage 0 charging. It was set to max at 6A, or 24% of the max output current.

Component	Equation	Calculated Value	Value used
R_{SENSE2}	$R_{SENSE2} = \frac{0.0497}{I_{OUT(MAX)}} \Omega$ [7]	2mΩ	10mΩ
R_{IMON_OUT}	$R_{IMON_OUT} = \frac{1208}{I_{OUT(MAXS0)} \cdot R_{SENSE2}} \Omega$ [7]	100.6kΩ	100kΩ
R_{IOW}	$R_{IOW} = \frac{24.3k \cdot R_{IMON_OUT}}{R_{IMON_OUT} - 24.3k} \Omega$ [7]	32.032kΩ	32.1kΩ
R_{IOR}	$R_{IOR} = 3.01k\Omega$ [7]	3.01kΩ	3.01kΩ
C_{IMON_OUT}	A C_{IMON_OUT} capacitor in the range of 4.7nF to 22nF is adequate for most applications. [7]	10nF	10nF

Table 2.2.6: Output Current Regulation Loop Equations and Values

After designing the input and output voltage and current regulation circuits, the rest of the design was based on the LT8490 datasheet. The full circuit schematic can be seen below in section 2.2.5.

2.2.2 Input Voltage Sensing

One more sub-circuit was added to scale the input voltage down to 3.3V so that it could be read by a GPIO pin on the ESP32 on the Inverter PCB. This subcircuit can be seen below in figure 2.2.7.

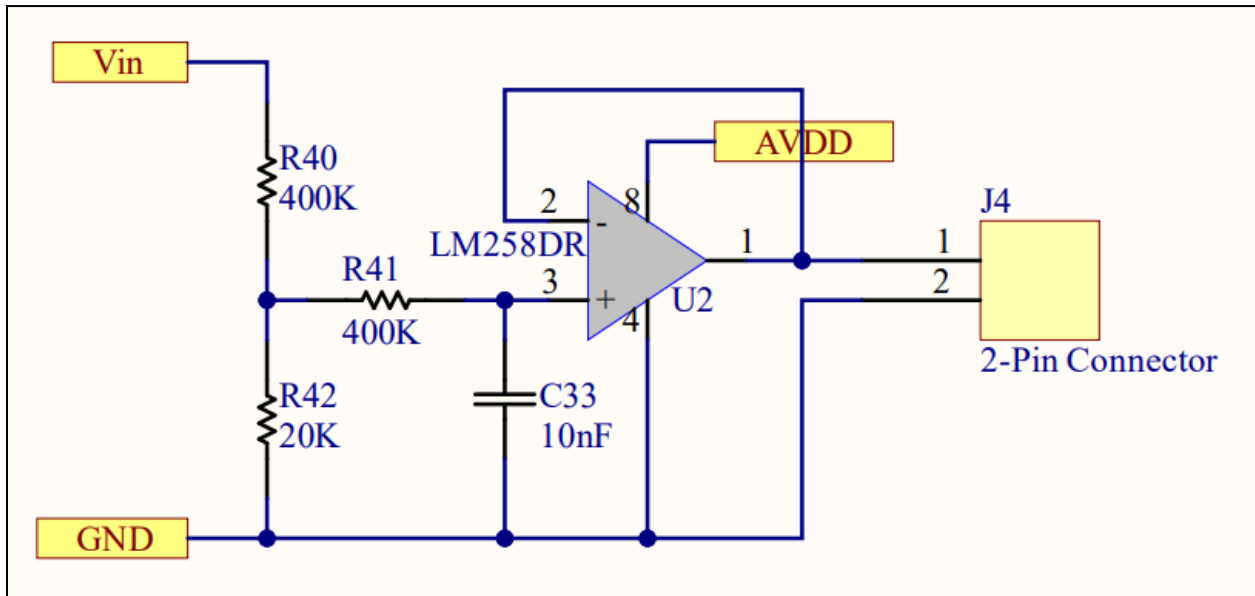


Figure 2.2.7: Input Voltage Measurement Subcircuit

The voltage divider between R40 and R42 has the following transfer function:

$$\frac{V_{output}}{V_{input}} = 0.047 \quad \text{Equation 2.2.1}$$

This is to ensure that the max voltage remains under 3.3V, the max input for a GPIO pin on the ESP32. R41 and C33 form a low pass filter to block any signals above 40Hz. Finally, the op-amp is used as a buffer to ensure that this subcircuit doesn't pull too much current away from the controller.

2.2.3 PCB Design

Below is a picture of the charge controller PCB. There are no components on the bottom side, so it is not shown.

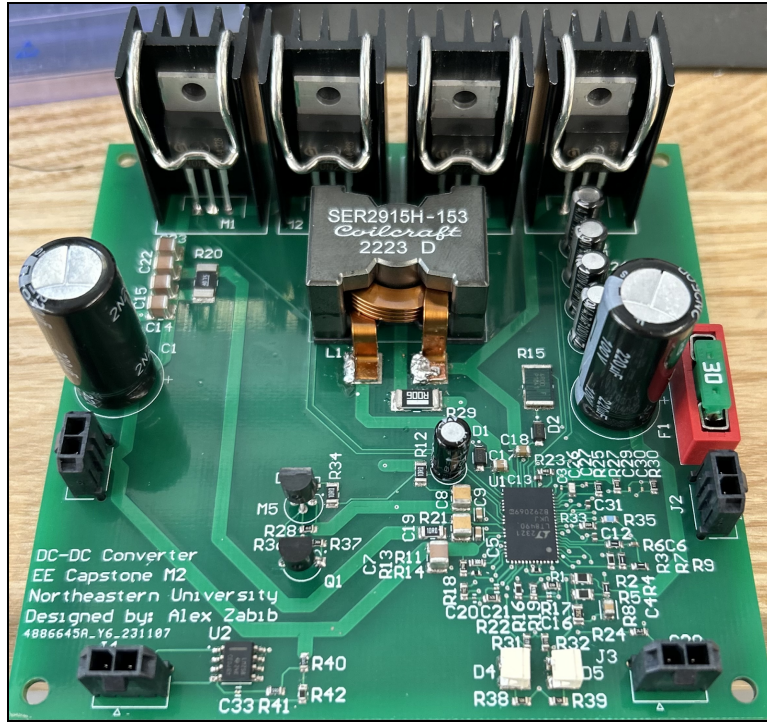


Figure 2.2.6: Top View of the Charge Controller PCB

The charge controller is a two-layer PCB and the design was centered around the LT8490. The bottom layer consists of some signal routing, but mostly a large ground plane. Because the LT8490 is a small chip with a lot of interconnections and components surrounding it, the layout of the components around it mimicked the layout of the DC2069A, the demo board for the LT8490 IC, to save time during the design process. Smaller components were also used to bring filtering capacitors closer to the IC. Thinner traces were used to connect to the IC and low power connections. For power signals to the IC, thick traces were used until they neared the IC. The LEDs were placed towards the edge of the board so they can be more easily seen.

The components used in the 4-switch buck boost were placed towards the top edge of the board so there would be more space for thicker traces, due to all these connections being higher power. The MOSFETs were rated for 250V and thermally coupled to heatsinks, to minimize the heat produced by the rapid switching of the MOSFETs.

All connectors were placed on the outer edges of the board to make wiring to the rest of the system easier. The input connector and input voltage sensing connector were placed on the left side of the board, along with input capacitors and input current sense resistor. The output connector and thermistor connector were placed on the right side of the board, along with output capacitors, the output fuse, and output current sense resistor. This made trace routing and wiring inside the electric box a more seamless process. Additionally, a throughhole fuse holder was added to the board to make replacing the fuse of the board easier if it was shorted.

2.2.4 Testing

To test the PCB, R13 was removed from the PCB to pull VINR to ground allowing us to connect a DC power supply to the input instead of solar panels. This was done to ensure that the PCB could take

an input voltage, and the LEDs would blink the correct error messages. For the second test, R13 was placed back on the board and a potentiometer was placed in series with the power supply so we could mimic the maximum power point tracking capabilities of the LT8490 IC when connected to a solar panel. The battery was connected to the output along with a 200W lightbulb in parallel to act as a load. The third test was to connect the solar panels to the input of the charge controller and see if the battery could be charged.

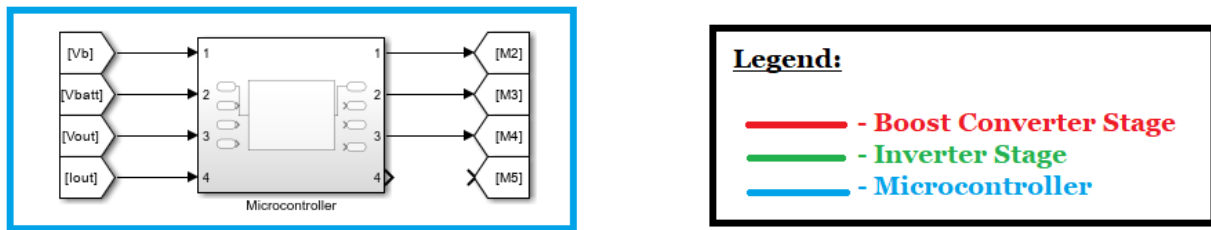
2.2.5 Full Charge Controller Schematic

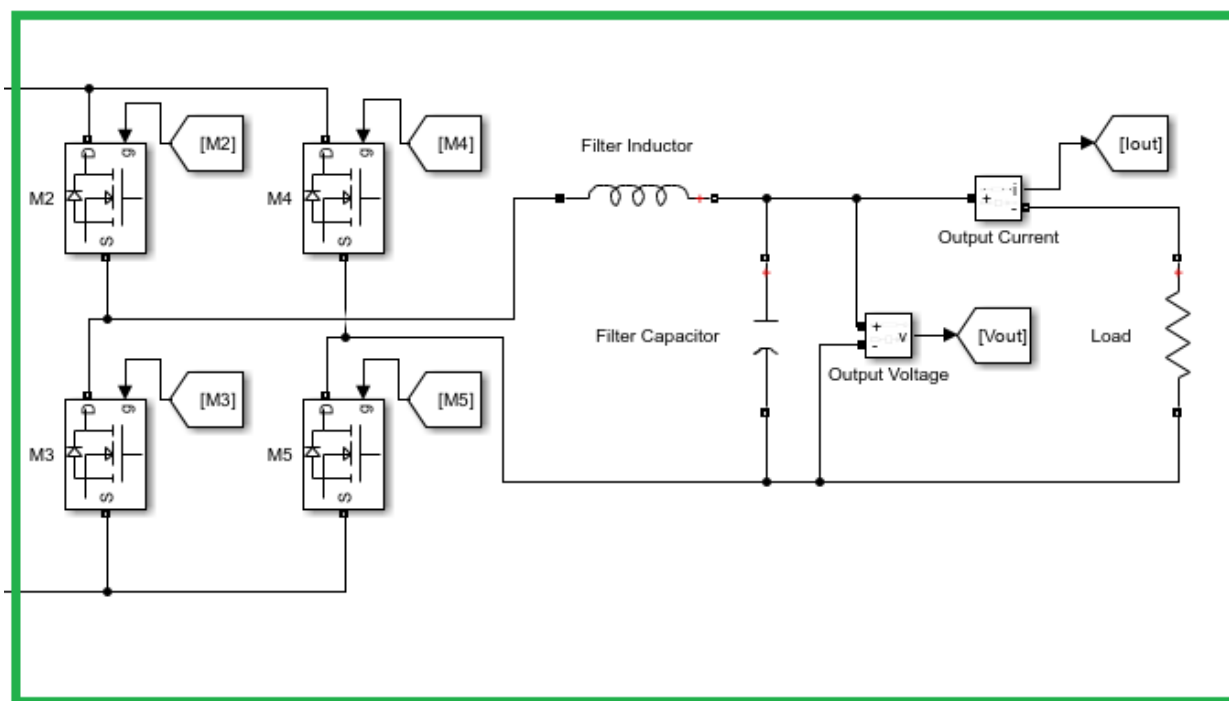
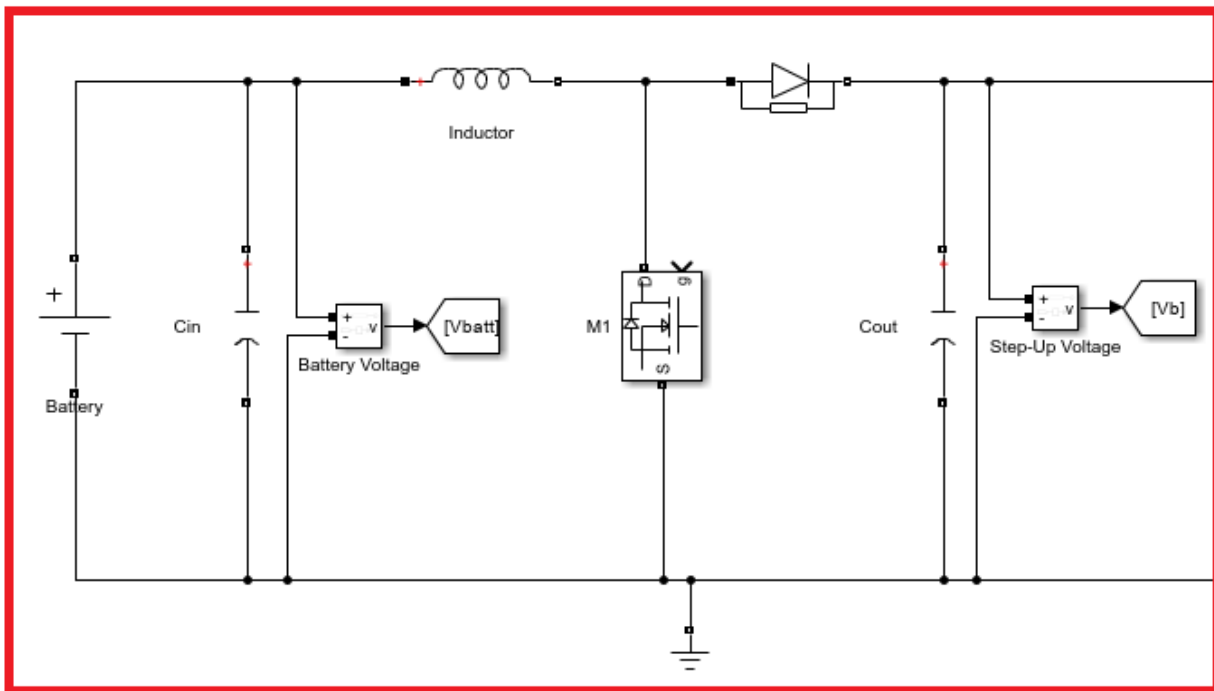
[DC-DC Converter Schematic.PDF](#)

This file is attached as a PDF because it is fitted for larger paper.

2.3 2-Stage Inverter

An inverter is designed to draw from a DC source and use a combination of switches to generate a square wave signal with a desired peak voltage and frequency, then apply filtering to smooth out the voltage and current to produce a sine wave that can be fed into an AC load. In this design, the source will be the internal battery of the system, and the load will be the e-mobility. The inverter will be made up of two stages (separate from the charge controller), essentially two converters cascaded to one another. The goal of the design is to take the 48 VDC battery at the input, step it up to 170 DCV, and output a 120 VAC. The controls for the boost converter will be managed by an IC controller while the inverter will be regulated by an MCU, and the device will be rated for up to 300W, as this is the typical rating for a power adapter that is used to charge e-mobility devices. [9]





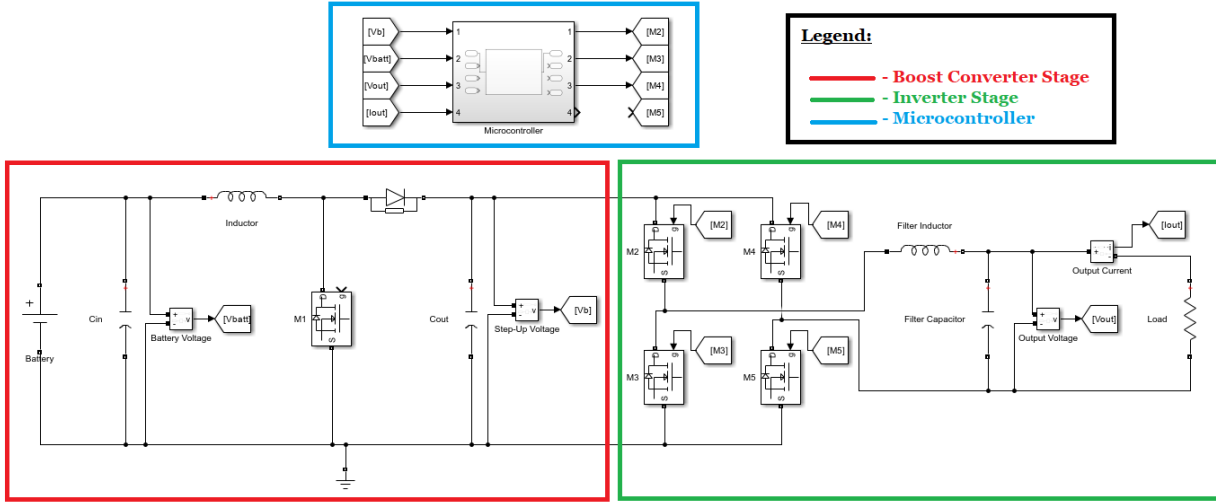


Figure 2.3.1: Simple Schematic of Inverter System

2.3.1 Boost Converter Stage

The topology for the first stage DC/DC will be a boost converter. As seen in the figure below, it is composed of mosfets and diodes for switching, an inductor to store and release energy, and a capacitor to smooth out the resulting voltage. [10]

The approach for component selection for the boost stage was for it to meet design requirements as well as be over-rated for the system's voltage and current values. The first stage is a boost converter (figure 2.3.1) that is capable of stepping up the voltage of the battery to 170VDC and is controlled by an LM5022 IC controller from TI (figure 2.3.4). The battery has a nominal voltage of 48V but fluctuates from 36V to 55V based on its charge profile. Thus the IC was chosen to include a feedback loop that could stabilize the output at 170V across the line regulation of the converter. The controller, input capacitors, and few IC resistors and capacitors (used to program the IC controller) were rated based on the max input voltage coming from the battery, whereas the remaining components, notably the inductor, diode, MOSFET, and output capacitors, were rated based on the output voltage of 170V. The maximum current in this system is 6.25A, thus all components are rated for this. The major components for this stage, the inductor and capacitor, are selected to minimize the voltage and current ripples in the system; 22uH and 69uF are their respective values.

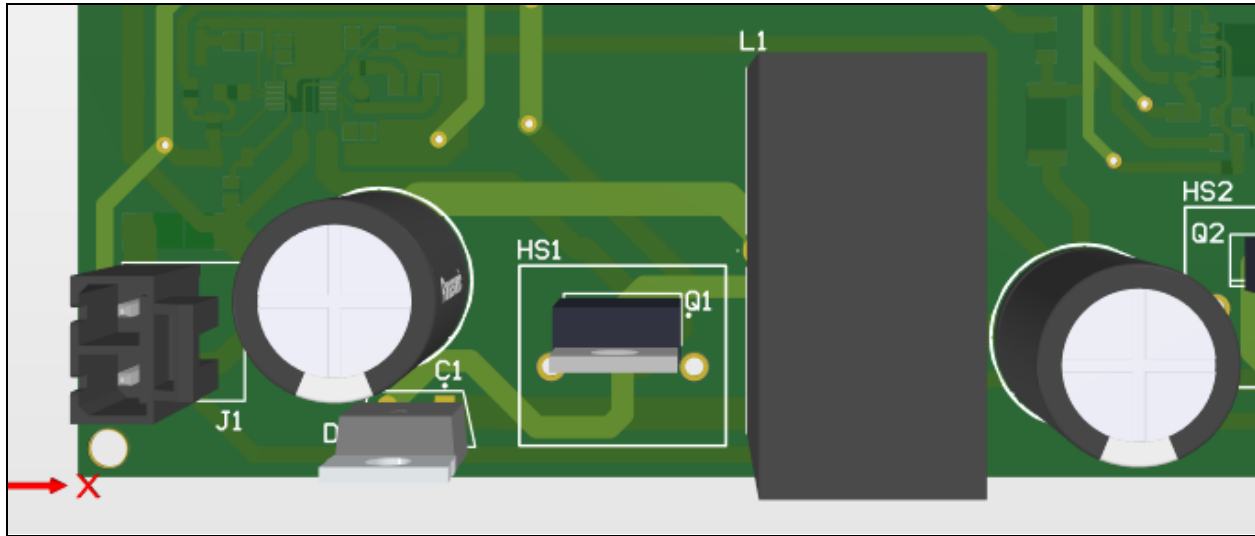


Figure 2.3.1: Boost Converter 3D Model and Schematic

2.3.2 Inverter Stage

The second stage is an inverter stage made up of a MOSFET H-bridge followed by an LC filter. The control scheme for the inverter is called a Unipolar Sinusoidal Pulse Width Modulation (SPWM) topology. How it works is that 2 modulating signals are fed into the MOSFETs. Looking at the H-bridge above, M2 and M5 share the same signal, while M3 and M4 share an opposing signal. This is so the switches are never on at the same time, otherwise a short will occur. The 2 modulating signals can be seen in the figure 2.3.2 below, which produce a moving average that is in the shape of a sine wave. The switching frequency of the MOSFETs is much greater than that of the 60Hz desired signal. Thus by applying this waveform to the LC filter, which is designed to attenuate high frequencies, only the 60Hz moving average shall pass and be fed to the output. Though the PWM generates many unwanted frequency components, in addition to large harmonics that extends to even higher frequencies which can interfere with the circuit communications, sensors, and digital logic, as long as the filters are designed properly then this interference can be managed and attenuated. [10]

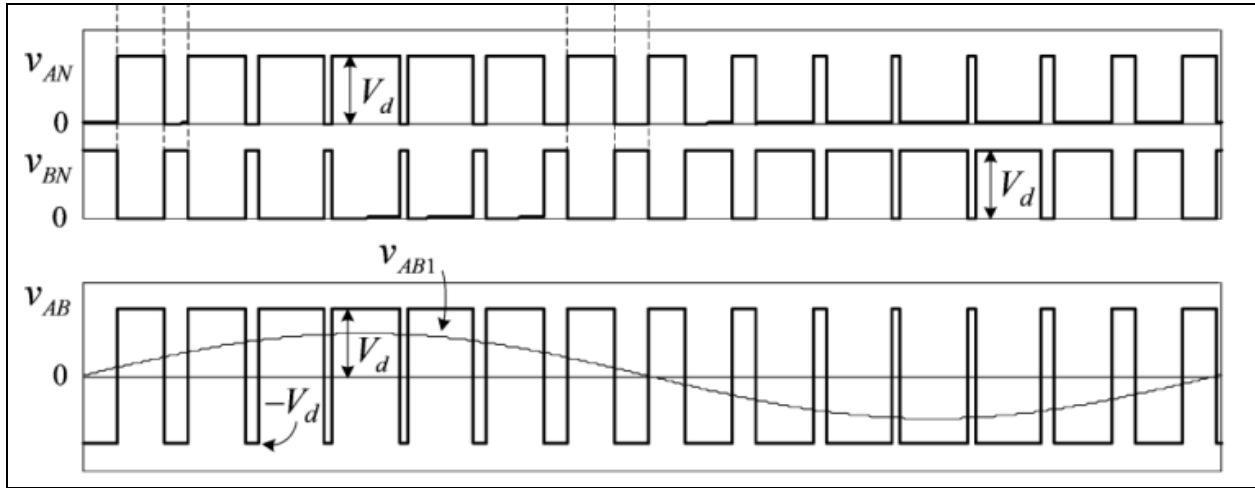


Figure 2.3.2: Current and Voltage outputs of a VSI (top plot) and PWM Inverter (bottom plot)

The same MOSFET type used in the boost stage is applied on the H-bridge. As for the filter, it is paramount that the current and voltage ripple be minimized as much as this will result in a smoother sinusoidal waveform. As a result, they yielded larger inductance and capacitance values when compared to the boost stage, with 4mH and 110uF as the values. The inverter's H-bridge is controlled by the ESP32 MCU. Because the MCU can only output a max voltage of 3.3V, a gate driver (UCC27712QDRQ1) is interfaced between it and the MOSFETs in order to step up the voltage of the modulating signal to 12V (as seen in figure 2.3.6).

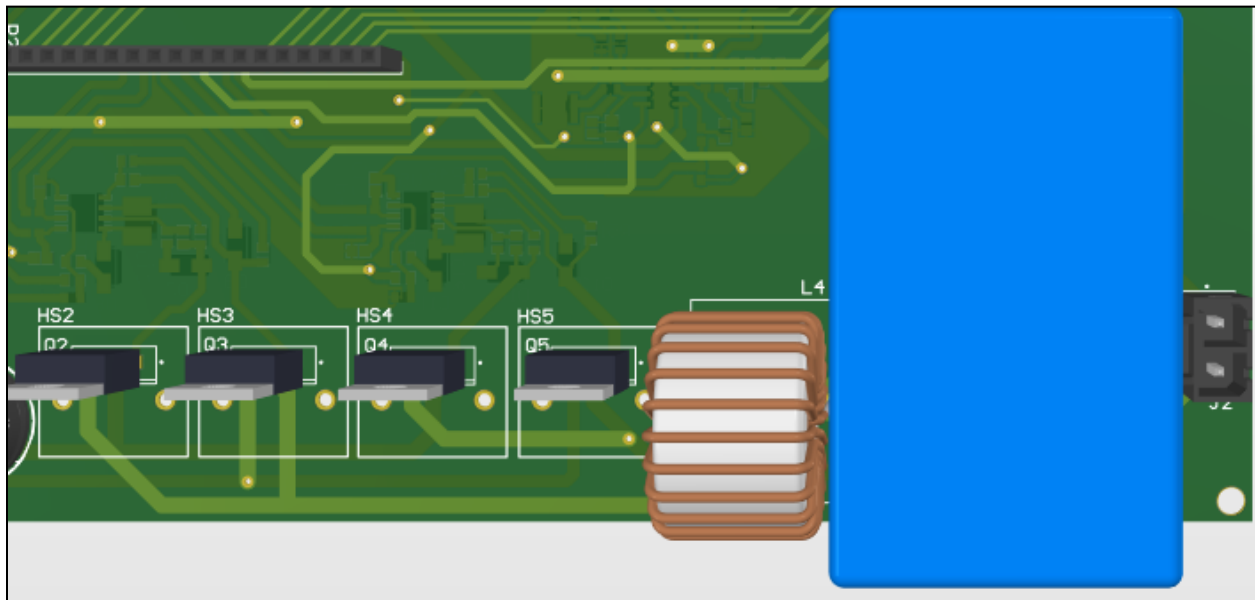


Figure 2.3.2: Inverter Stage 3D Model

2.3.3 PCB Design

Before proceeding to the layout, many other supporting components, systems, and considerations had to be implemented on the design. Two safety aspects were implemented in this design: thermal dissipation and high voltage spacings. Each stage is split into two parts, the power stage and the control scheme. The power stage is the part of the layout that observes the maximum voltage and current of the system and consists of the connectors to interface with the board, power semiconductors, and filtering components (inductors and capacitors). Since the design deals with voltages as high as 170V, we are required to comply with clearance and creepage standards; respectively IPC-2221 and IPC-9592. These standards pertain to the distance between high voltage traces on a PCB. If these traces are placed too close, arcing could occur. After referring to these standards and creepage/clearance distances, we calculated a value of 5.6mm minimum between traces and pads. As such, the components and traces were spaced to comply with these spacings, as were the pads of the components, particularly the connector where its pitch clearance (space between contacts) was selected to slightly exceed the required 5.6mm spacing. This was done for voltage protection, but for current protection fuses were implemented on the input and output to address any shorts that occur on the board. The standard for fuses are based on IEC 60269, stating fuses be placed on the input and output of a switching converter. Then on the thermal side, heat sinks were implemented on the MOSFETs. Because these switches operate at a high frequency, they face the most amount of stress among the components, and thus are considered failure modes with the shortest lifetime. To mitigate this degradation, heat sinks are implemented to dissipate heat to the ambient environment. In addition, a fan was used to cool the ambient temperature around the components. The fuses and heat sinks can be seen in the final layout in figure 2.3.7.

Other support components include the power regulators, voltage/current sensing circuits, MCU header pins, and ferrite beads. The power regulators, seen in figure 2.3.3, were fed by the input voltage, supplying 12V and 3.3V logic voltages to other components. 2 voltage divider circuits, consisting of precision resistors, measured the input and output of the boost converter, feeding them to the MCU. In addition, measurements of the output voltage and current were regulated by an Op Amp circuit that filtered out unwanted frequencies and stepped down voltage to near logic levels so it could be fed to the MCU (seen in figure 2.3.5). The output voltage was measured simply from the output connector while the current was measured by a current transformer implemented outside of the board and converted to a 1V AC signal; fed in by a 3.5mm audio connector. Additional header pins allowed one to interface with unconnected pins of the MCU for troubleshooting. Lastly ferrite beads addressed signal integrity on the control side; mitigating high frequency noise on the traces and stabilizing the path. [11]

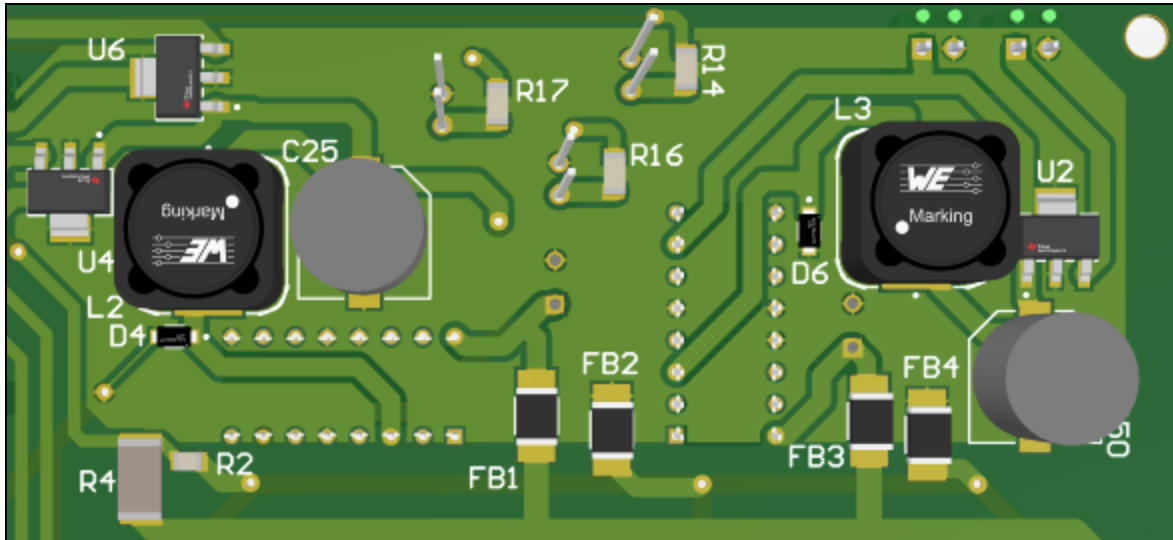


Figure 2.3.3: Power Regulators 3D Model

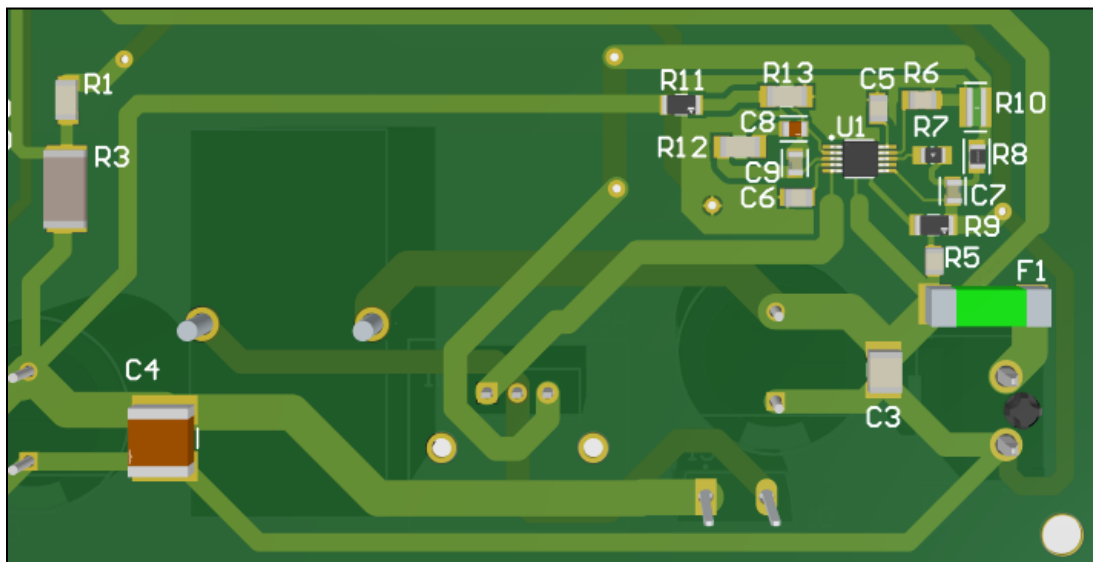


Figure 2.3.4: Boost Converter IC Controls 3D Model

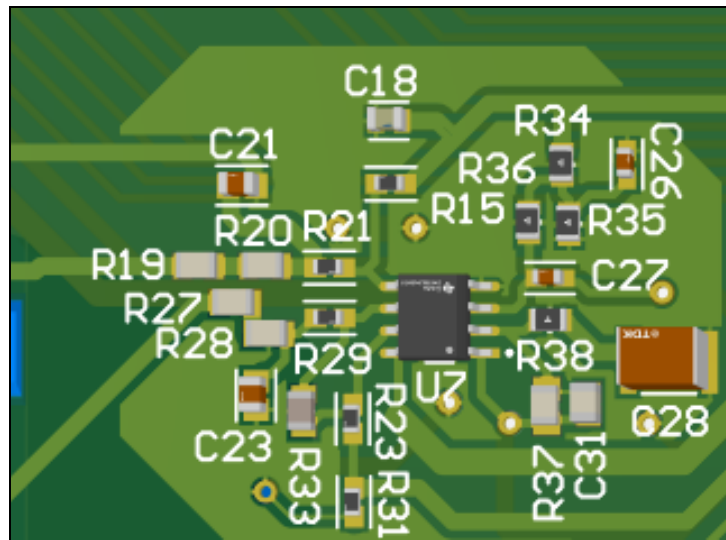


Figure 2.3.5: Output Voltage/Current Measurement Circuit 3D Model

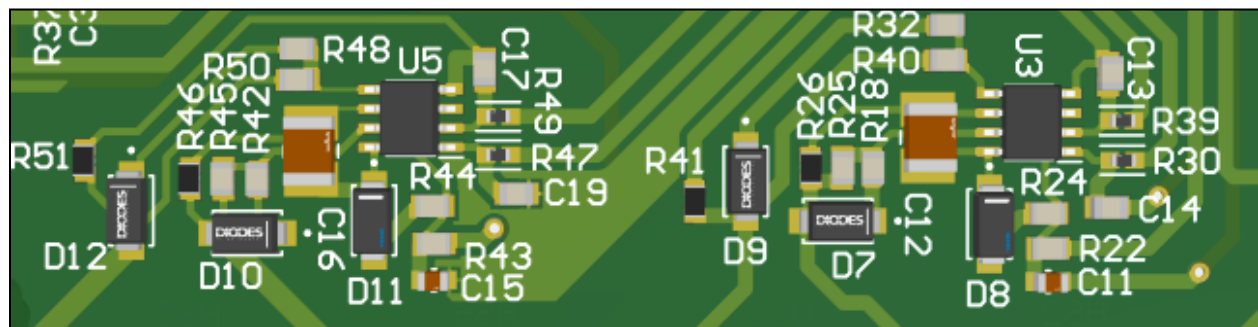


Figure 2.3.6: Gate Driver Circuits 3D Model

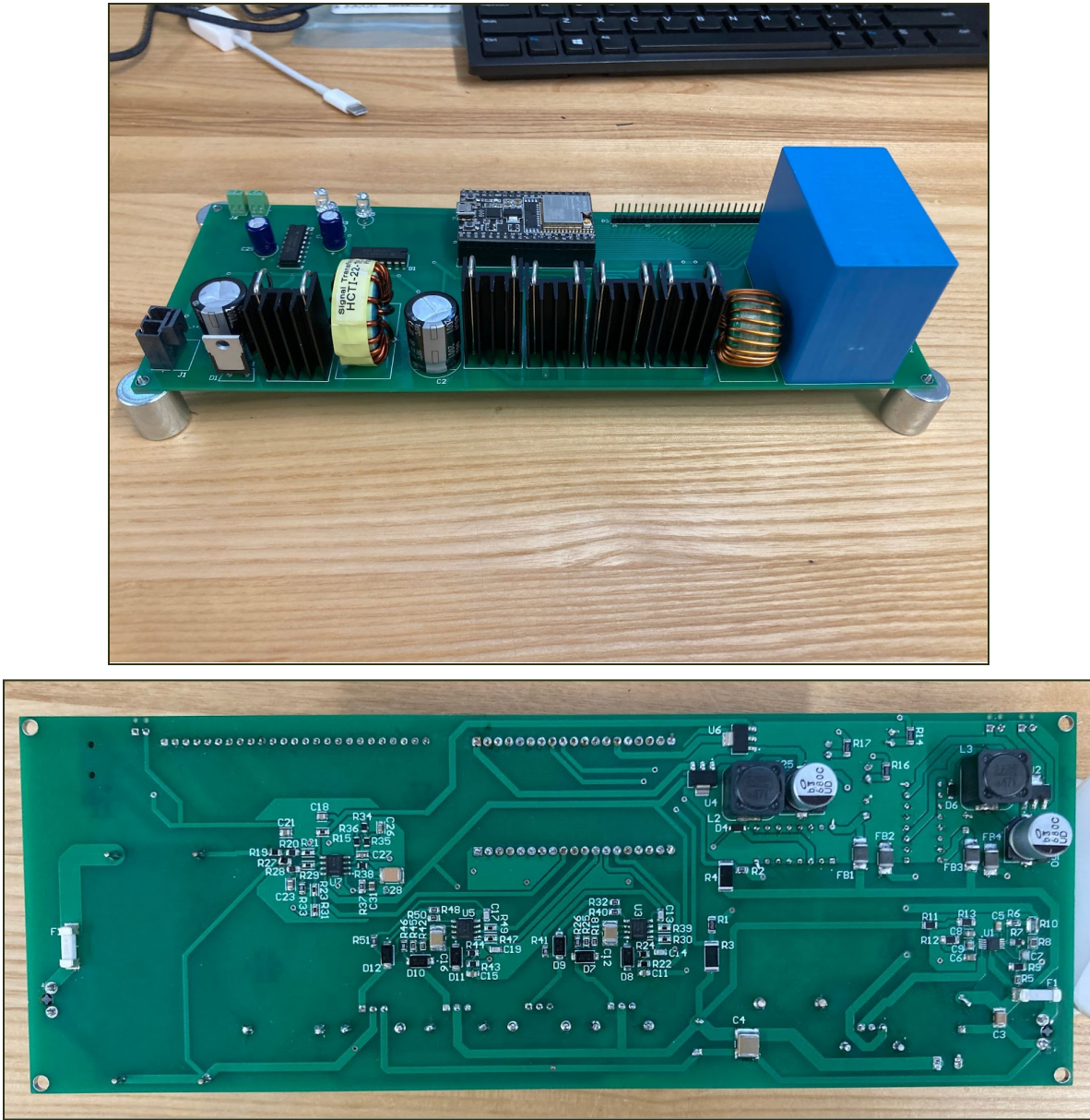


Figure 2.3.7: Finalize PCB Layout of Top Layer (Top) and Bottom Layer (Bottom)

2.3.4 Testing

The testing procedure here involved observing the open circuit behavior of each individual stage of the inverter. Starting with the boost stage, the input voltage was incremented slowly starting at 20V and increasing to the max voltage of 55V. At 36V, the boost stage began to output 170V, prior to this it matched the voltage of the input. This is a feature of the IC controller when its input voltage is low compared to the output. Then a supply voltage of 50V was fed to the input of the inverter stage and switching was done to achieve a sinusoidal output; lower than the 170V as this was initial testing. The regulators were observed throughout testing to assure they produced the desired 12V and 3.3V. When

supplying a load at the output of the inverter, the measurement voltages and currents were recorded on the MCU to assure the inverter operated properly. The load here was a 200W incandescent light bulb.

2.3.5 Full Inverter Schematic



Inverter_Schematic.PDF

This file is attached as a PDF because it is fitted for larger paper.

2.4 Software Ecosystem

The development stack combines the versatility and speed of Flutter, a cross-platform framework, with the robustness of MQTT, a lightweight messaging protocol, to enhance mobile application functionality. The integration of these technologies orchestrates a seamless and responsive communication infrastructure between the mobile application and two ESP32 microcontroller units housed within the enclosure mentioned above.

2.4.1 App Development

The primary framework for application development was driven mainly by the need for cross-platform development. This shortened the playing field a bit, with two competitors standing out amongst the rest: React Native and Flutter. Though React development is well documented thanks to the immense community behind the framework, Flutter holds an advantage in both performance and development time. “Ahead of Time” (AoT) compilation and the use of native languages rather than compiling from Javascript within Flutter gives it the edge in performance. Additionally, development time is also known to be faster on Flutter thanks to the library of widgets that give the developer access to most tools necessary for creating a user interface. The built-in tools along with Flutter’s hot reload feature, which allows the screen to reload without relaunching the entire application, greatly increased the development time of this application. Lastly, because this was done by a single developer, the single codebase for multi-platform development helped to maintain order within the repository, better manage debugging, and optimize resources as no additional time would be needed to develop an application for a different platform (ie. web, android, macOS).

With the decision to use Flutter, came the adoption of Dart as the backbone of this project. Not only were we new to Flutter as a development tool, but no member of the team had any experience in Dart either. However, Dart shares similar syntax to C++ with a few added features by Google, so syntax and a few basic programming projects sufficed for the learning phase for Dart. Next, navigating the Flutter framework posed its challenges, with the framework’s swift evolution causing online tutorials and even official documentation to become outdated within a short span of six months. To gain familiarity with the toolkit, the example “Hello World” app was used along with a Dart/Flutter LSP to trial-and-error test some features while reading through the beginning documentation. After achieving basic comfort building a screen, the objective became developing a basic app with the Google Maps Flutter API integrated within the home screen. The API produces a map, which is crucial to the final application design. Shockingly, this, or more specifically integrating the map along with a user-location feature, proved to be a multiple-week endeavor.

The projects mentioned above all served to show the capabilities of Flutter and to develop a user interface. Once the difficulty of various designs became more obvious, the final app could be more comfortably designed to accommodate a timeline. Each element of an app in Flutter is known as a screen, three of which were made for this project: map, station, and list_stations. The resulting design can be seen in the figure below.

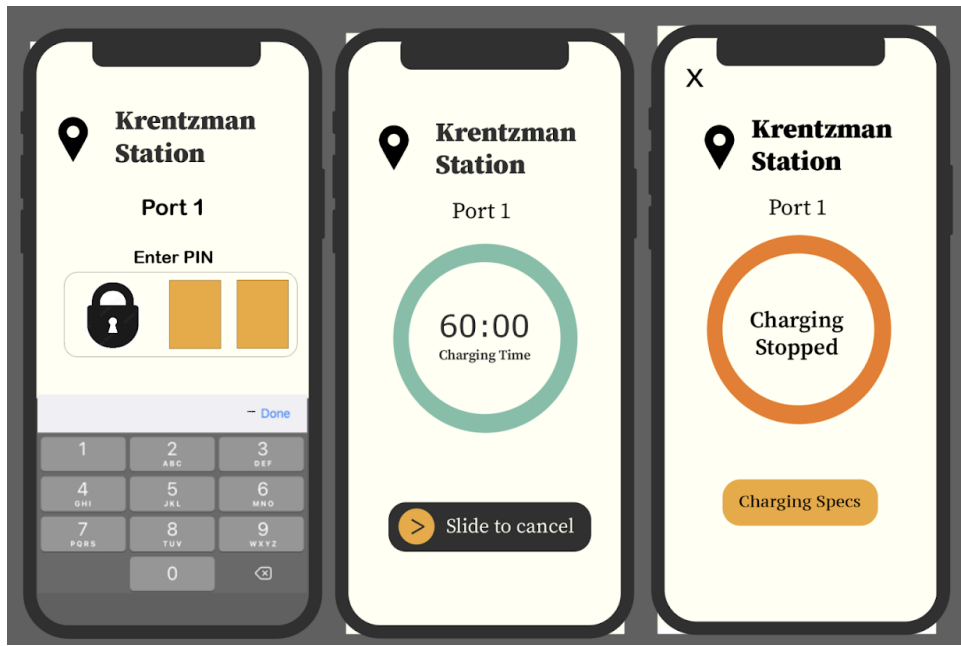


Figure 2.4.1: Final UI design

The development phase commenced with the creation of data models to represent the underlying structure of the application. Models were created for map, to initialize the pin locations for each station's location on the map, and for station, to more easily access metadata about each station such as ID and number of ports. Following this, the screens were implemented, adhering to the predefined UI layouts. The process was relatively smooth, with minor inconveniences arising on the locally downloaded version of the application in preparation for demo day; however, the errors were quickly fixed and the UI was updated to be more dynamic based on screen size. The last step was the integration of MQTT, which included creating a secure connection with an MQTT broker, more on this later, to send and receive messages to and from specified topics and subtopics.

The intentional structuring of the repository and thoughtful design of UI layouts, combined with the efficient execution of data models, screens, and MQTT integration, produced a cohesive and functional application. Many thanks to the countless GitHub tutorial repositories that helped guide me through the structure of Flutter applications, which proved essential in calming the chaos that is Flutter repositories.

2.4.2 Microcontroller Software Development

The decision to employ ESP32 microcontrollers for this project was primarily propelled by their versatility and notably low power consumption, aligning seamlessly with the project's IoT requirements.

Leveraging ESP32's built-in Wi-Fi capabilities, robust processing power, and support for various communication protocols, the microcontrollers proved to be an ideal choice.

In the software development phase, the first ESP32 was designed for effective charge state management using a software-based Pulse Width Modulation (sPWM) waveform. The primary goal was to optimize the control of output charge from an outlet connected to our electrical enclosure, specifically for charging e-mobility devices. The sPWM algorithm, crafted for precise waveform generation, offered a versatile method for toggling charge states while ensuring efficient and controlled power delivery.

Simultaneously, the second ESP32 was tailored to generate secure Two-Factor Authentication (2FA) codes, aligning with the project's commitment to robust security. Specialized algorithms were implemented to ensure dynamic and secure code generation. The integration of a seven-segment display served as a visually accessible output for the generated codes.

Both ESP32 units were designed for MQTT communication to relay their charging states and generated 2FA codes, as well as to receive requests from the user-application to enable/disable charge and to generate the 2FA code. This design choice not only streamlined communication but also reflected a holistic approach to efficient charge management.

2.4.3 Messaging Protocol

The communication protocol between the microcontrollers and the user application was initially intended to be facilitated through AWS IoT Core, utilizing the MQTT protocol for seamless message exchange with the IoT MQTT Broker. However, recognizing the potential increase in both cost and development time associated with AWS IoT Core, an alternative solution was sought to maintain efficiency without compromising functionality.

As a strategic decision, we opted for a customized setup using Eclipse Mosquitto MQTT broker, hosted within a Docker container on a secured EC2 instance. Leveraging the free tier version of AWS EC2 instance, this solution provided a cost-effective infrastructure for the project. The EC2 instance was rigorously locked down, permitting communication solely through port 1883. Within this secured environment, port forwarding was configured to redirect the Docker container's port 1883 to the corresponding section on the EC2 instance. Access to the MQTT broker residing in the Docker container was regulated by requiring initiation through a specified username and password system. This approach not only capitalized on the cost savings offered by the AWS free tier but also allowed for a tailored and secure communication infrastructure. The combination of the microcontrollers and the user application proved seamless, underscoring the inherent simplicity of the MQTT protocol, which facilitated efficient communication between the components.

2.4.4 Development Process

The development process for this project followed a structured and collaborative approach, utilizing version control through GitHub to manage code repositories for the ESP32 microcontrollers, Flutter application, and simulation code generated from Simulink/MATLAB. Each component's codebase was housed in its respective repository within the main GitHub repository, ensuring organized version

tracking and collaboration among team members. This centralized version control approach facilitated seamless coordination, allowing for efficient monitoring of changes, collaborative contributions, and the ability to revert to previous states if needed. [12]

2.5 Scaled System Simulation

It is necessary to establish a grid connection for this system to be scalable and reliable for the user. The prototype was not connected to the grid due to coordination with the local utility company and other authorities having jurisdiction, a process that can take months or years. A simulation was created to demonstrate how the system would perform if connected to the grid. The simulation allowed us to observe changes in the battery SOC, grid interconnection and synchronization, and power output under fluctuating load and weather conditions. Simulating this behavior allowed us to observe and analyze how the grid-tied inverter protects the charging station and enhances the overall usability of the system. The goal of the simulation was to show the system's ability to satisfy high loads, even under unfavorable weather conditions, by measuring the changes in supplied and demanded power of the various system components, including exporting excess power back to the grid.

The simulation was performed using Simulink, complemented with the Simscape Electrical Toolbox component library. Simulink is a programming environment that provides customizable block libraries for modeling, simulating and analyzing dynamic systems. This program is integrated with MATLAB, and can be integrated with a variety of toolboxes, depending on the purpose. Simscape Electrical was used to develop the proposed microgrid charging station, along with the connection to the grid. The toolbox is capable of analyzing the generation, conversion, transmission, and consumption of electricity in high power electrical systems. The only addition to the block diagram for our prototype's electrical system is the grid connection. To supply power back to the grid, the block diagram in Figure 2.6 includes net metering, and a grid-tied inverter. The high-level block diagram of our simulation is shown below. [13] [14]

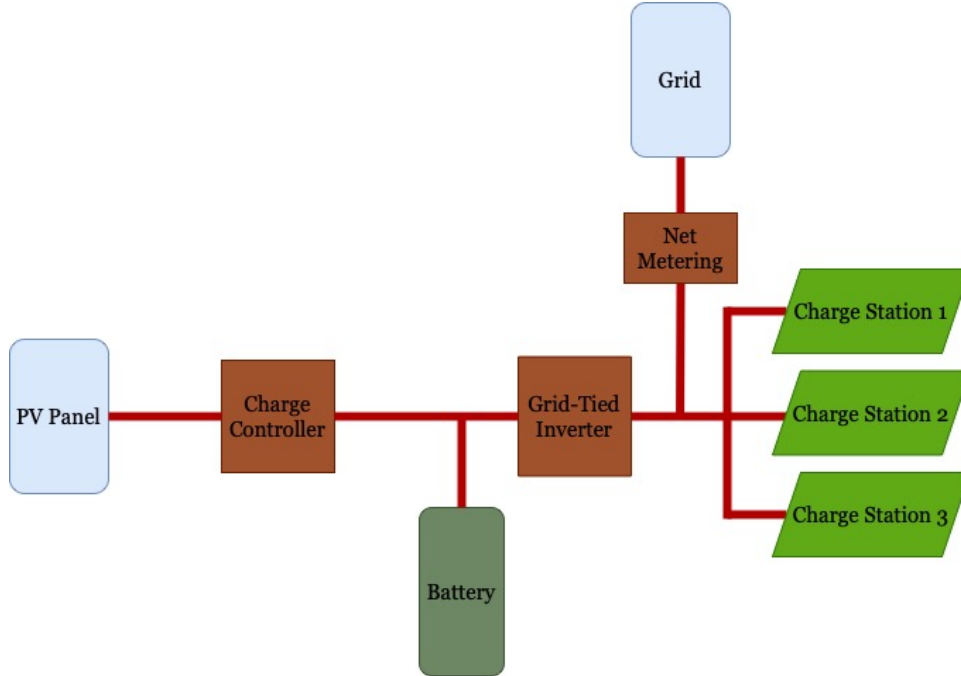


Figure 2.6: Simulink Model Block Diagram

2.5.1 Overview

Our system is divided into six different subsystems: (1) solar panels, (2) charge controller boost converter with maximum power point tracking, (3) battery, (4) DC-DC boost converter, (5) inverter with low pass filter, and (6) the grid and load. All of these subsystems were scaled to power a load of up to 10 e-bikes. Since we were establishing an interconnection with the grid, we followed IEEE Standard 1547 regarding synchronization parameters for interconnection to an energized area EPS. Table 2.5.1 shows the required percentages of difference between the nominal voltage of the grid and our results in the output of the simulated system. As will be presented further in our description, our results fall within these thresholds during the grid interconnection process.

Aggregate rating of DER units (kVA)	Frequency difference (Δf , Hz)	Voltage difference (ΔV , %)	Phase angle difference ($\Delta\Phi$, °)
0–500	0.3	10	20
> 500–1 500	0.2	5	15
> 1 500	0.1	3	10

Table 2.5.1: IEEE Standard 1547

The following figure 2.5.1 presents the overall topology of the simulated system. To analyze the system properly, an in-depth explanation of each subsystem is described in the next section.

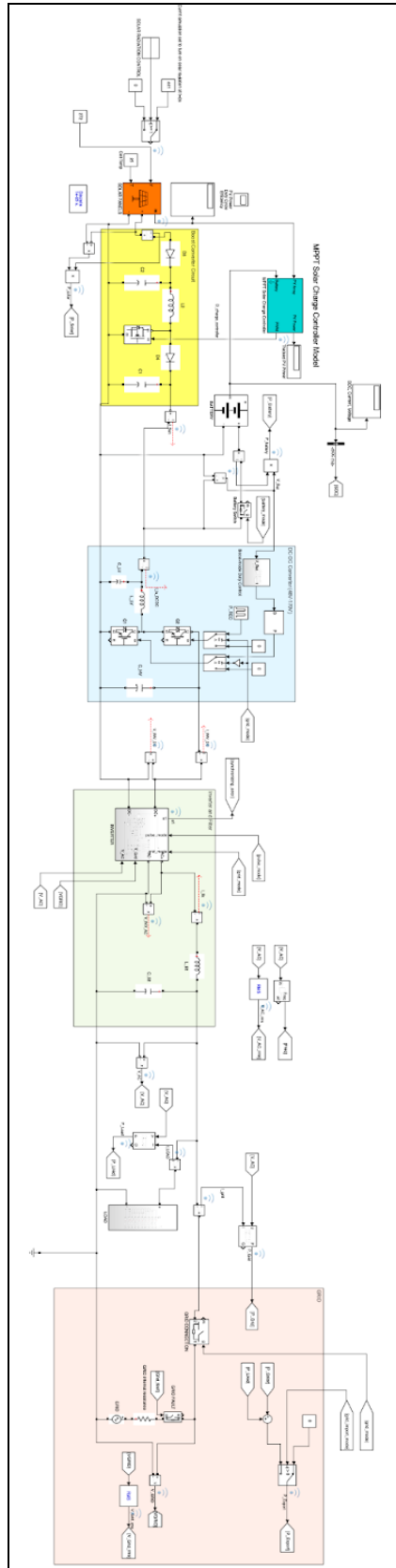


Figure 2.5.1 Overview Topology of the Simulation

2.5.2 Solar Panels and Charge Controller

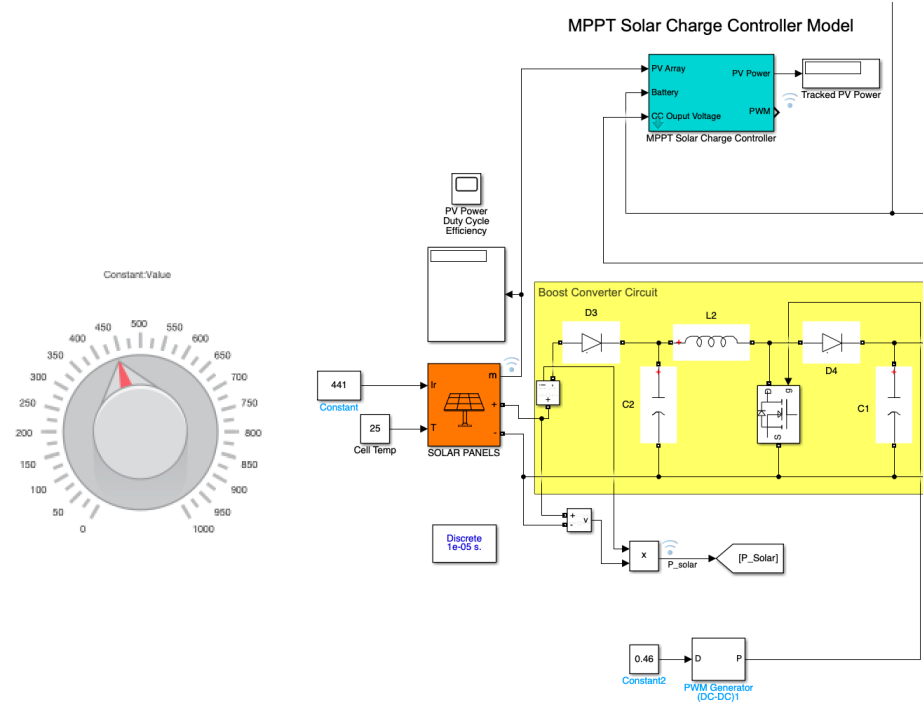


Figure 2.5.2 Topology of the Solar Panels and Charge Controller

To be able to provide enough power to 10 e-bikes at maximum irradiance, it was necessary to size the solar panels to output more than 1.25kW. To provide a reliable system, we decided to oversize the system to output 1.87kW in ideal conditions. Each solar module (Tesla Inc. SR24S3-2) had a rated power of 23.4W and a rated voltage of 3V. The modules were then arranged into 8 parallel strings of 10 modules per string. The output voltage of the solar array is DC at around 30V. The full current-voltage and power-voltage characteristics of our solar array are presented in figure 2.5.3. We also included the irradiance, which we could modify accordingly, depending on the weather conditions we wanted to test.

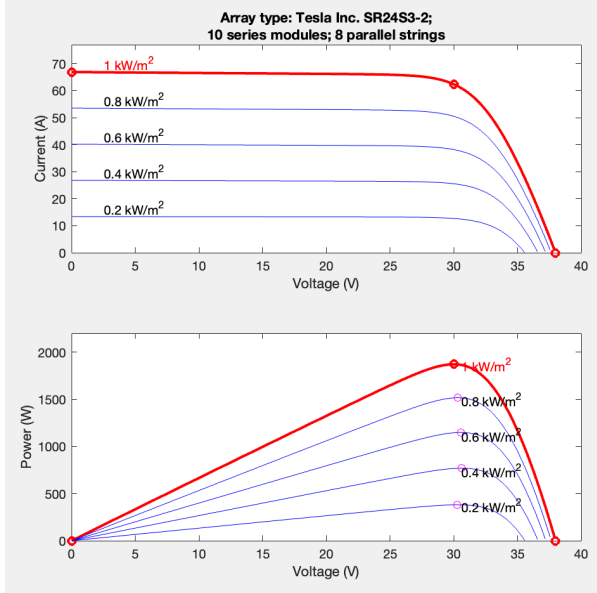


Figure 2.5.3 Specs of the solar array

To match our results as much as we could to reality, data was obtained from the National Solar Radiation Database. We observed the average and maximum values of irradiance over the summer and winter period in Boston during 2022 [18], the results were 981, 441, 742 and $271 W/m^2$ (GHI) [15] for summer maximum, summer average, winter maximum, and winter average, respectively[17]. These were the irradiance values we evaluated to validate our results. [16]

To optimize the efficiency of the solar panels and obtain the maximum power output, we implemented a MPPT algorithm in our charge controller. Its task was to adjust the operating power point and monitor the output of the solar panels to keep the system operating at or near the MPPT. This algorithm aided in the overall performance and effectiveness of the system.

We designed a boost converter to increase the voltage at the output of the solar panels to match the rated battery voltage. The output of the solar panels is 30VDC, and our battery had a rating of 48V, therefore we implemented a boost converter between these two subsystems to allow connection. The primary components of the boost converter include an inductor, a switch (in our case, an IGBT), a diode, and a capacitor. The duty cycle of the switch (the ratio of time the switch is closed to the total period) determines the output voltage. By adjusting the duty cycle, the boost converter can provide a regulated output voltage, even when the input voltage varies. In our case, the duty cycle was determined by the MPPT algorithm.

2.5.3 Battery and DC-DC Converter

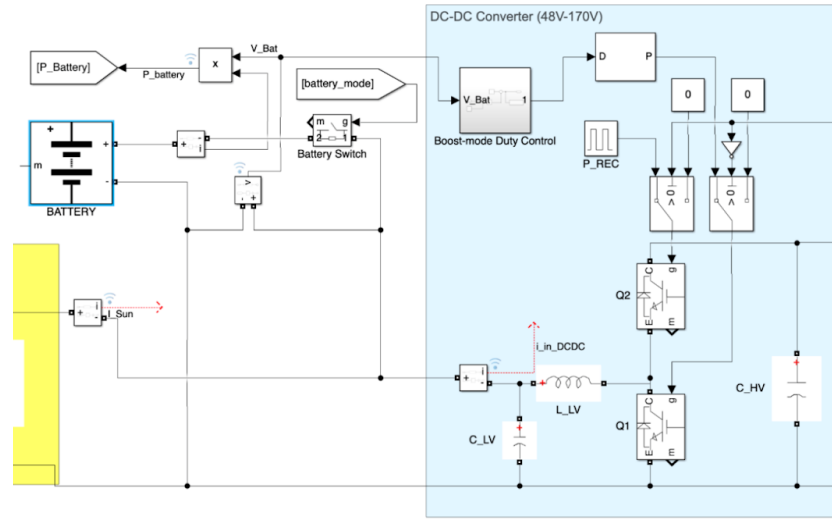


Figure 2.5.4 Topology of Battery and DC-DC Converter

The battery is capable of storing 3.84kWh, which on its own is able to provide continuous power for 10 e-bikes for over 2 hours. The battery connects to the output of the charge controller and the input of the DC-DC Converter. We also implemented a switch that controls when the battery is on or off. This is determined by the SOC and the connection to the grid, as the battery is turned off when there is excess power to be exported to the grid. The different modes of operation are described in section 3.5.4.

A DC-DC converter is introduced to boost up the voltage at the output of the battery, considering that this system would be connected to the grid, which in our case is rated at 170V peak. While not used in our simulation, this boost converter was designed to allow for bi-directional power flow if charging the battery was desired. In our case, we wanted to prioritize the use of renewable energy, so the battery is only charged from the solar panels and the reverse power flow feature (charging the battery from the grid) is not used.

2.5.4 Inverter and Filter

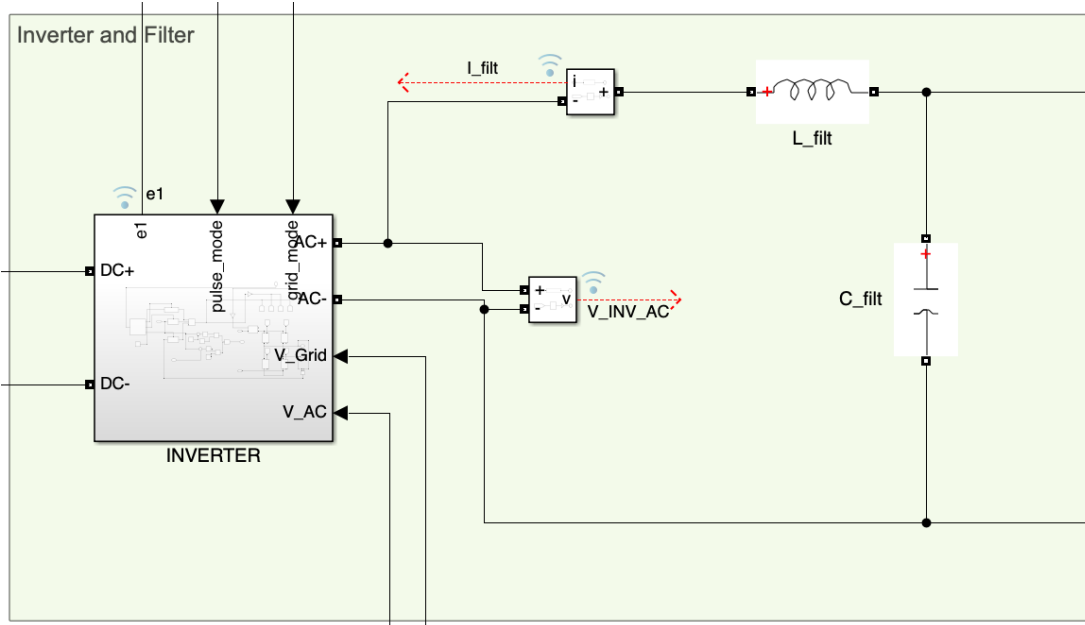


Figure 2.5.5 Topology of Inverter and Filter

The main purpose of the inverter is to convert the DC output of the DC-DC Converter into an AC voltage. The inverter circuit consists of a combination of IGBTs, controlled by the logic implemented to optimize the system and satisfy load demands. The DC input is switched on and off rapidly by the inverter circuit. This switching action, combined with PWM, creates a series of pulses. Through appropriate filtering and modulation techniques, these pulses are shaped into a sine wave or a modified sine wave, resembling the standard AC power waveform of the grid. We used an LC lowpass filter to remove the high frequencies introduced during the SPWM switching. The inverter is also responsible for handling the logic that determines the mode of operation of the system. A state machine with defined thresholds was created to switch between the various modes, and in each case, the inverter is modulated in a specific way to control the system behavior. There are 4 modes of operation in our system:

1. **Island mode:** In this mode, the system is not connected to the grid, and therefore is providing the power demands with the solar output and/or battery. The system will operate in this state when the battery SOC is greater than 20%. Once the SOC goes below that threshold, the system will transition to grid synchronization.
2. **Grid Synchronization mode:** The goal of our system is to provide power to the user even if there is not enough power coming from the sun or the battery is low in charge. To achieve this, we must establish the interconnection with the grid following appropriate synchronization parameters. This mode is the transition period between island and grid connected mode. The output voltage of the system must match in phase with the AC voltage of the grid to connect safely, therefore we designed an algorithm that synchronizes the phases accordingly by modulating the inverter with respect to the phase of the grid voltage. Once the waveforms are in sync, a connection with the grid can be established.

3. **Grid Connected mode:** Once the grid is connected, the power demanded at the load will now be supplied by the grid. In this case, if the solar panels are producing any power, it will charge the battery, however the power from the grid will only be used to charge the load. The system will remain in this mode until the battery reaches an SOC of 30%. This threshold was established to avoid a longer than necessary connection with the grid, as the battery could take a long time to charge if the weather is not favorable. Once the grid disconnects from the system, the state will transition back to island mode.
4. **Grid Export mode:** When the power from the sun is greater than the power demanded by the load, and the SOC of the battery is greater than 80%, there will be a surplus of power. This is what would be considered the power exported back to the grid measured with net metering. Our system calculates this value when the battery goes above 80%, at which point the battery is disconnected. The threshold of 80% was chosen as an optimal normal operating limit to avoid overcharging and improve the health of the battery over its lifetime. Once the supplied power is no longer in excess (due to increased load or decreased power from the sun), the system will transition back to island mode and power will be supplied by the solar panels/battery.

2.5.5 Grid and Load

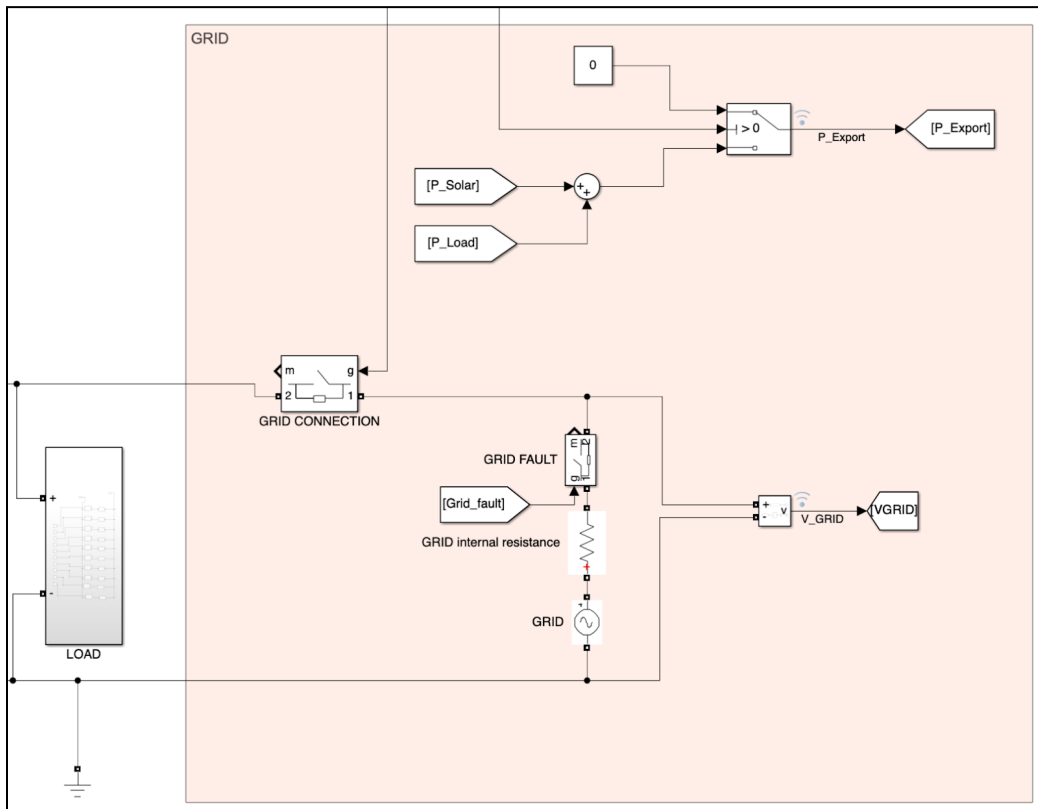


Figure 2.5.5 Topology of Load and Grid

The grid was modeled using a simple 170V peak amplitude AC source, along with a resistor to model the internal grid resistance. Two switches were implemented to enable or disable the grid. The grid fault switch is meant to model any abnormal behaviors on the grid such as line faults. The grid connection switch is controlled by the inverter logic, enabling or disabling according to the state the system is in.

The load is modeled using a combination of multiple resistors, each meant to represent an average power demand from one e-bike, equivalent to 120W. We gave the system the capability of controlling the load connection while the simulation was running by use of toggle switches. This was to study the behavior of the system while it is operating and a new load is introduced or disconnected, as it would be in the practical environment.

2.6 Prototype Efficiency

The table below lists the efficiency of each of the subsystems and the total system efficiency. For the mechanical system, this was determined by estimating losses in components such as the wiring terminal connections, and solar panels. The efficiency in the charge controller and inverter were calculated based on the switching and conduction losses of the MOSFETs, which contribute the most energy loss out of all the components of a switching converter. Lastly the battery's efficiency was taken straight from its data sheet.

Subsystem	Efficiency
Mechanical System	95%
Charge Controller	98%
Inverter	99%
Battery	98%
Total System	90%

Table 2.6.1: System Efficiencies

3 Project Planning

3.1 Timeline



Figure 3.1: Gantt Chart

Figure 3.1 shows the Gantt chart for our project from when initiated the design process through the final presentation of the prototype in December 2023. The Gantt chart is color coded by each part of the project, the charge controller, inverter, mechanical design, app development, two-factor authentication and simulation. Visualizing the major task groups and their phases this way is very effective for allocating time to different components of the project and adjusting what we need to be focused on at any given time as things come up. The planning phase for each task group took place for the majority of September. The

period from early to mid-October, was dedicated to designing each of the tasks. Testing of each part took place separately until mid November. The final integration of the system took place through the rest of November. The final prototype was presented the first week of December. Throughout the entire design process, documentation of engineering design choices and changes took place to maintain a comprehensive record of decisions and resources.

3.2 Task Breakdown

The following chart represents a simple task breakdown by each group member.

Assignee	Task	Sub-tasks	Co-Assignee
Ali	Inverter	Schematic Capture	
		PCB Design and Assembly	Alex
		Power Measurement for Feedback Loop	
		Thermals	
		Voltage/Current Sense	
		Communication with AWS	Michael
Alex	Charge Controller	Schematic Capture	
		PCB Design and Assembly	
		Power Measurement for Feedback Loop	
		Thermals	Ali
		Voltage/Current Sense	
		Two-Factor Authentication	Michael
Ezekiel	Mechanical Design	Spec Solar Mount	Ali
		Spec Electrical Box	Alex/Ali
		Load connections and grounding (other harnessing too)	Alex/Ali
		Security for AC adapters	Michael
		CAD Design	Valentina/Grady
		Designing cooling options for electrical box	Ali
Grady	Project Management	Research/Inquire about project proposal report requirements and create report template	Valentina
		Keep Gantt up to date/monitor progress of tasks	
		Document project scope and objectives (for proposal report)	ALL
		Track project expenses/monitor budget	
		Document design decisions and modifications	Valentina

Michael	User notification & GUI	GUI Development	
		ESP32 sPWM generation (w/ Voltage/Current data)	Ali
		MQTT integration and setup	
		AWS security management	
		2FA with app using ESP32	
Valentina/ Grady	Simulation	Acquire solar irradiance data sets from PVSam	
		Research model for charge controller, inverter, battery and grid	
		Design algorithm for grid interconnection	Ali
		Create plots of simulation outputs	
		Research Safety Standards for grid interconnection	Ali

Table 3.2: Work Breakdown Structure and Task Assignment Chart

3.3 Resource Allocation

For successful execution of our project, available resources were allocated efficiently. Our multidisciplinary team comprised members with expertise in electrical engineering, software development, and project management. Electrical engineering-focused team members were responsible for designing and integrating the electrical components of the station, including solar panels, battery, charge controller, and inverter. Software-focused team members were responsible for developing the app-based user notification system, integrating communication hardware, and developing the grid-connected simulation model. Project management and team leader responsibilities included overseeing the project timeline, allocating resources, and coordinating among team members. Refer to Table 3.3 for a comprehensive breakdown of project work and team member task assignments/co-assignments.

The necessary equipment and materials included solar panels, a battery, charge controller infrastructure, inverter infrastructure, connectivity modules, and structural components including an electrical box and panel support apparatus. The bill of materials in section 5 of this report goes into more detail on required physical components for this project. Additionally, major software necessary for completing this project included CAD software and Matlab Simulink and the Simscape Electrical toolbox. The total budget of the project was \$685. Figure 3.2 includes a breakdown of how much of the percentage was allocated to each part of the project. Necessary software licenses required for this project are provided with Northeastern University. By thoughtfully allocating these resources, we ensured that each aspect of the project was well-supported in terms of time, human resources, and money.

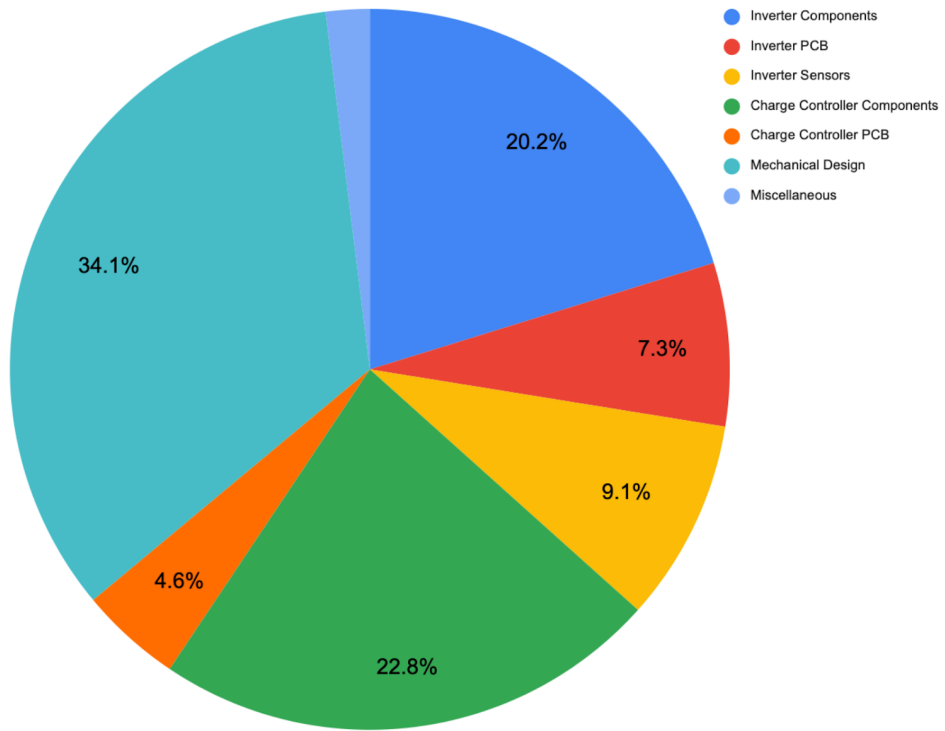


Figure 3.2: Pie Chart of BOM

General BOM	
Breakdown	Costs
Inverter	\$250.86
Components	\$138.53
PCB	\$50.11
Sensors/Thermals/Other	\$62.22
Charge Controller	\$187.11
Components	\$155.86
PCB	\$31.25
Mechanical	\$233.45
Miscellaneous	\$13.47
Total:	\$684.89

Table 3.3: Bill of Materials

3.4 Communication

To increase the success of our project, communication channels and meeting frequency of our team were defined during project initialization. Communication planning allowed us to stay on target by providing weekly updates to our advisor, defining short-term and long-term goals, and providing different channels for communication to improve efficiency and access to information. Discord was chosen as the primary means of communication via messaging. This server was used to create different folders, each containing information about tasks individually. Discord is an easy-to-use platform, which allows for quick exchanges of messages between relevant team members and organization of important links and resources. Google Drive was chosen as the hub for all project related files. This includes reports and presentations regarding the project as a whole as well as charts and diagrams for specific components. Additionally, weekly meeting notes are housed on Discord for easy reference and updating.

All-team meetings with the faculty advisor were set weekly for forty five minutes. These meetings were allocated to provide updates and receive feedback from our advisor. Additionally, a weekly internal meeting without our advisor was scheduled once a week to identify and assign tasks, collaborate on relevant parts of our project, and discuss ways of incorporating feedback from our advisor. Further meetings were scheduled throughout the week as deemed necessary, and smaller meetings between relevant team members were held to work out tasks where major project components overlap or where members are assigned to collaborate on a specific project component.

4 Results

4.1 Mechanical system

The implemented mechanical system met performance and reliability expectations aligning with the intended objectives outlined in the project. The design optimized solar energy generation at 42° and emphasized features like durability, safety, security, and ergonomic maintenance access. The concrete base, serving dual roles as an anchoring weight and an elevation platform, strategically lifted the solar array to an ideal height mitigating tampering risks.

Moreover, the electrical enclosure designed in strict accordance with NEC standards, successfully housed the electronic components securing the entire system against any potential tampering threats. The grounding system, utilizing a three-parallel ground rod setup within a horticultural substrate, has been enhanced for optimal conductivity, adhering to the safety regulations outlined within the National Electrical Code. This approach significantly minimizes the risk of electrical shock, solidifying the system's commitment to safety and reliability.

4.2 Charge controller

The first stage of testing consisted of removing R13 on the charge controller, to set the LT8490 in DC Power Supply mode. Then, a power supply set to 15V limited at 0.8A was connected to the controller. The LEDs were observed to see if an error message would be shown. The LEDs indicated that there was no load connected to the output, and this was the expected result. The 48V Lithium-Ion battery was then connected to the output and the LEDs indicated that the controller was in the second charging stage. This was expected because the battery was charged above 98%. In the figure below is the reading of the power supply at 15V, a reading of the input voltage scaled to have a 3.3V max on the orange multimeter, and the voltage of the battery on the multimeter on top of the oscilloscope. A lightbulb was connected in parallel with the battery to act as a load.

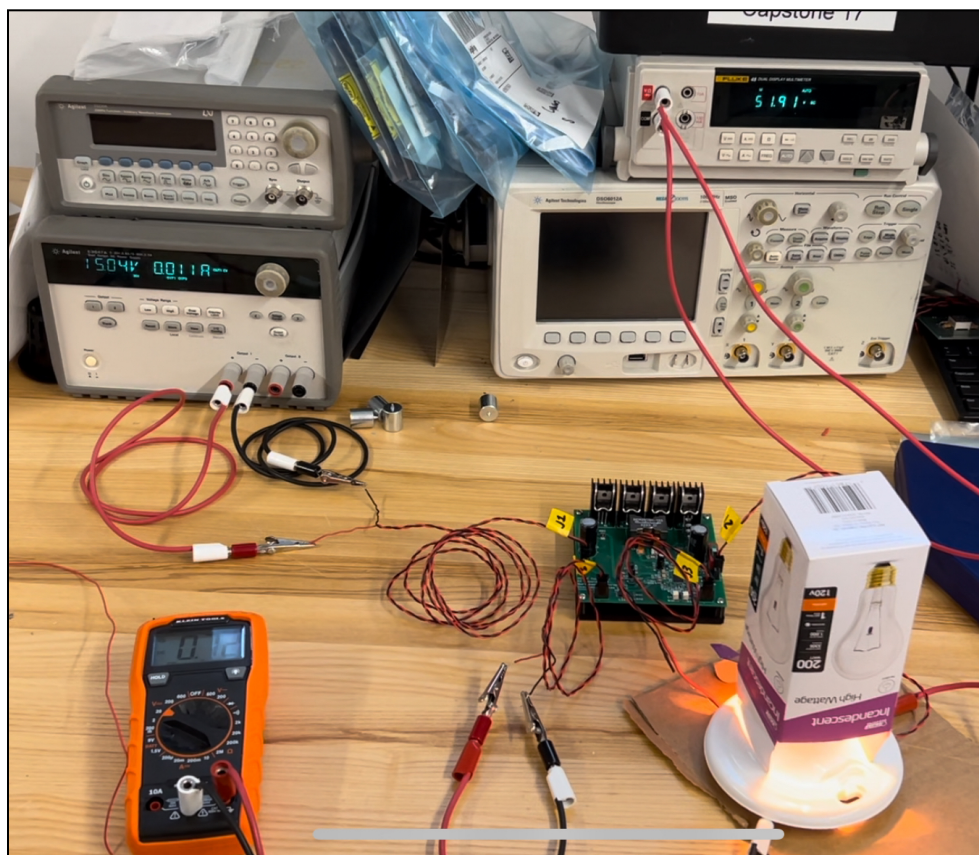


Figure 4.2.1: Testing Set-up for the Charge Controller

A potentiometer was then placed in series with the power supply to mimic the maximum power point tracking that the LT8490 would implement when in solar power supply mode. When the input voltage and current was changed the voltage at the output and the charging state did not change, which was the desired output.

4.3 2-Stage Inverter

During testing of the inverter, a manufacturing error was found where one of the traces and pads began to touch one another. This caused a short in the system and prevented any further testing from occurring. However, testing prior to the fault showed that the boost stage functioned as desired. In addition testing was done on the ESP32, which was responsible for producing the modulating signal. By filtering out the signal, we acquired a moving average sine wave at 60Hz, as seen in the figure below.



Figure 4.3.1: Filter Waveform of Modulating Signal

4.4 Software Ecosystem

Our system seamlessly integrates the Flutter app with ESP32 microcontrollers, featuring a robust software-based Pulse Width Modulation (sPWM) for precise charge state control. The app serves as a user interface, allowing users to verify Two-Factor Authentication (2FA) codes, connect to a station at a specified port, and enable charging for e-mobility devices such as e-bikes and e-scooters. The user-friendly Flutter interface enhances accessibility, providing clear controls for efficient and straightforward interaction. The images below give a concise visual overview of the final app state, showcasing these key functionalities.

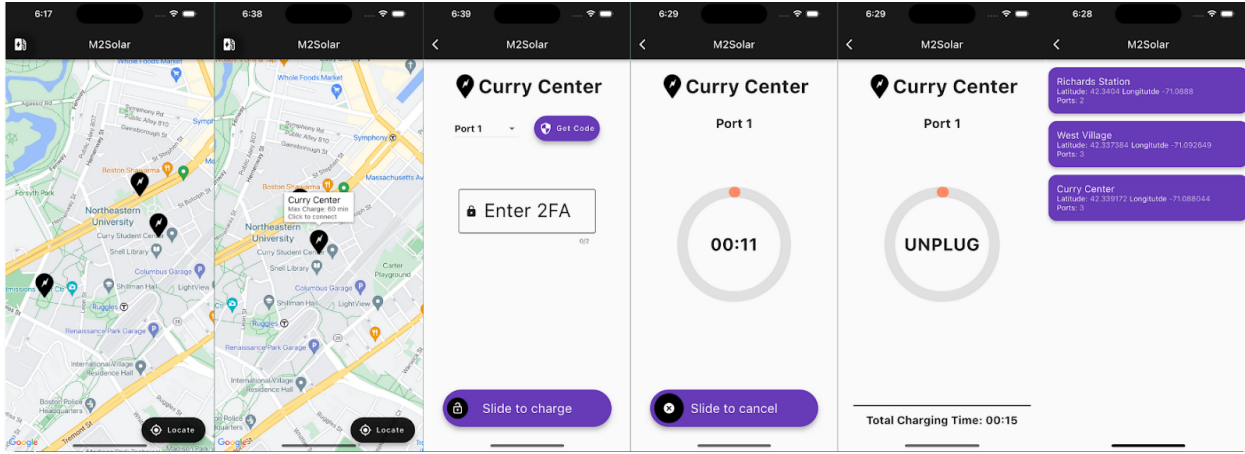


Figure 4.4.1: Final Capstone Application built with Flutter

4.5 Simulation

The simulation was performed multiple times with different conditions, meant to show how the system would work on the different modes. As noted in the design description, the average value for irradiance in Boston during the winter is $271W/m^2$, this was the first irradiance input irradiance tested. Figure 4.4 shows the output plot of power vs. time. The simulation was run for 4 seconds, and the initial state of charge of the battery was set just above 20%. Once the simulation started, the battery was charging with the solar power, and there was a load demand of around 1.3kW. Once the battery is at an SOC below 20%, the voltage is synchronized with the grid around 3.1s, a connection is established and it supplies the full power to the load. The battery proceeds to charge with the output power from the sun. This figure shows the system in three different operation modes, island, grid synchronization and grid connected.



Figure 4.5.1 Simulation Power Results with Grid Interconnection

Figure 4.5.2 shows a plot of the state of charge of the battery vs. time. We can see that as soon as the battery goes below 20%, it starts charging with solar power. This can also be compared with the power plot above to see how the charge and discharge of the battery plot coincides with the time at which the grid connects.

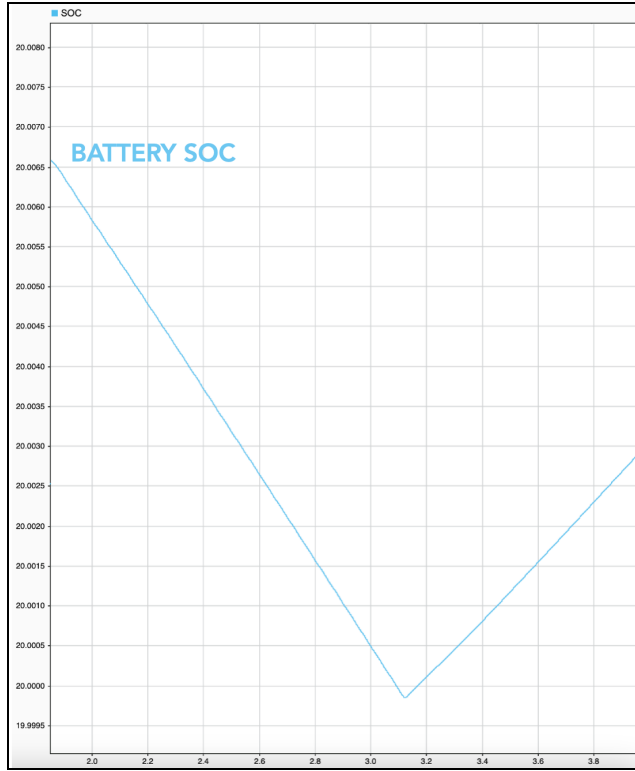


Figure 4.5.2 Simulation SOC Results with Grid Interconnection

To model the voltage of the output of the inverter and the grid voltage, we created a voltage vs. time plot. Figure 4.5.3 shows the simulation screenshot of the point in which the inverted is between island mode and synchronization mode. As we can see, once synchronization starts, the output voltage starts to fluctuate unevenly. This is due to a transient response of the system, and occurs for a very short period of time, around 3 cycles. Once the system processes the new modulation scheme, we observe how the voltage aligns with the AC waveform of the grid. Once the two are considered to be matched, well within the requirement of IEEE 1547, the system connects with the grid at the next zero crossing.

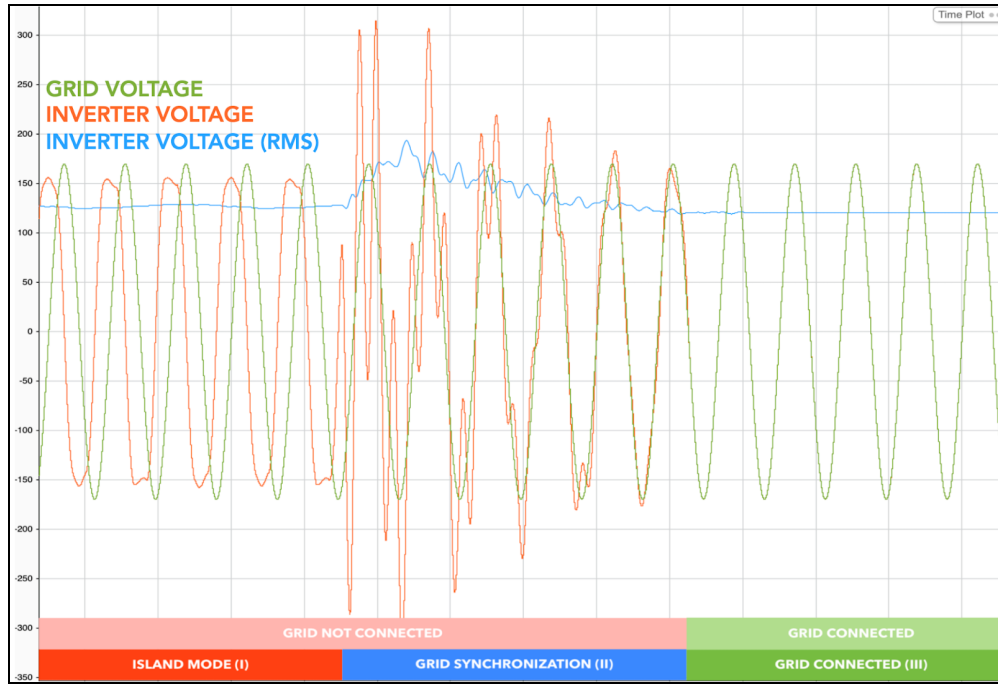


Figure 4.5.3 Simulation Results of Voltage Synchronization with Grid Interconnection

The following plot in Figure 4.5.4 shows the system operating in island mode only. In this scenario, the irradiance was set to the max recorded in Boston in 2022, 981W/m^2 the battery has an initial SOC of 50%, and at each second of the simulation, the load was increased.

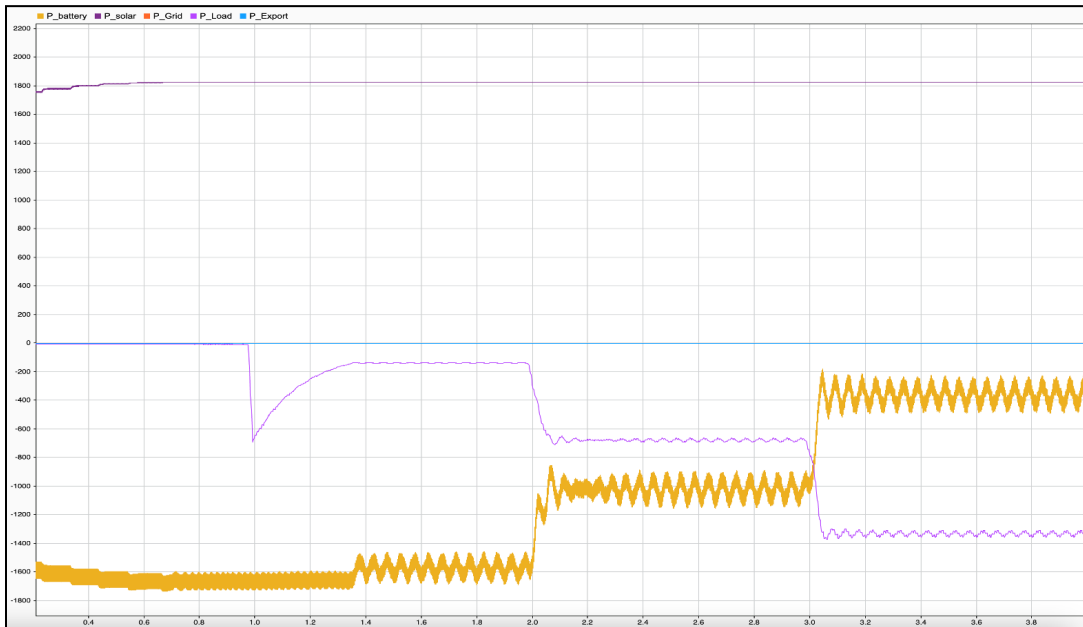


Figure 4.5.4 Power versus Time during Island Mode

As we can see, the power coming from the grid is always 0W, the load demand is increasing at every second, and the battery absorbs power throughout the run. The battery power comes closer to 0

every time an additional load is connected. This is due to the fact that the system prioritizes sending power to the load rather than to the battery. In this scenario, the power coming from the sun is enough to power up to 10 e-bikes and charge the battery at the same time at 400W.

We also tested the system under the various irradiance conditions stated in section two. The resulting power behaviors are similar to those shown in Figure 4.5.4, however in some cases, the power generated by the solar panels is not enough to cover the load, and the battery must transition from demanding power (charging) to supplying power (discharging). Figure 4.5.5 illustrates an average of the battery charging rate (in %SOC/hr) under the various irradiance and load conditions. It should be noted that these charging rates are linearized around 50% SOC, however, this assumption may not hold as accurately when the battery is below 20% or above 80%.

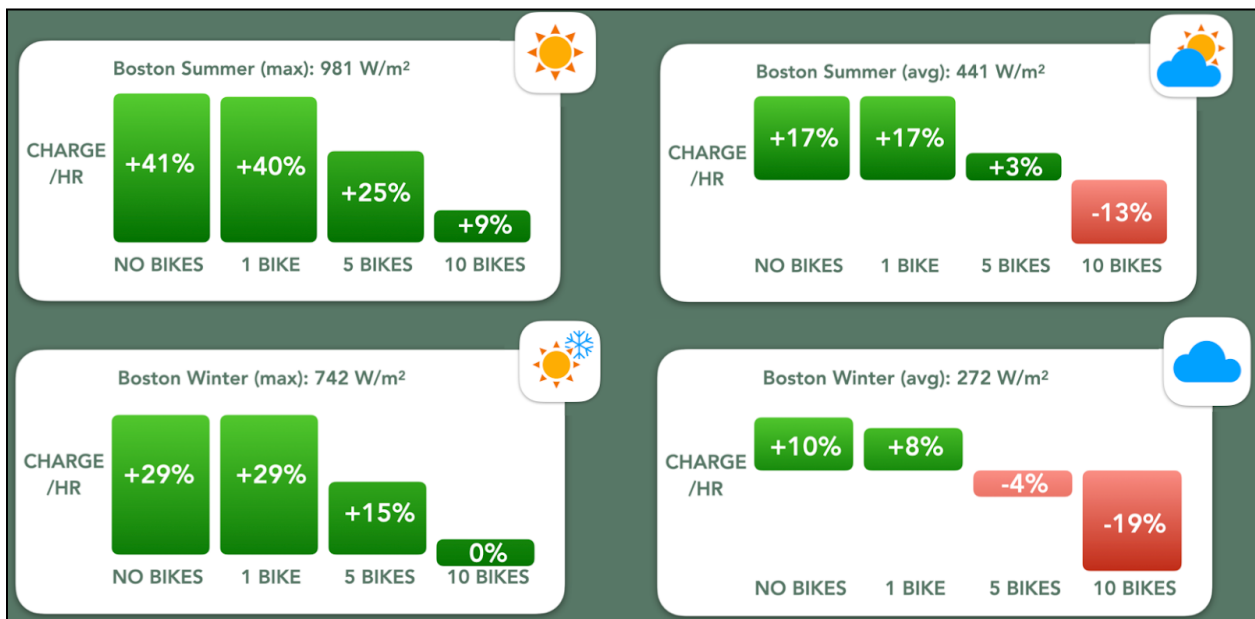


Figure 4.5.5 Battery Charge Rates for Various Irradiance/load Conditions

The last scenario demonstrated was the mode in which the system is producing surplus power, which is considered the power exported to the grid. Figure 4.5.6 shows the power vs. time plot of this simulation run. At this point, the system is in grid export mode. The initial state of charge of the battery was 85%, the irradiance was set to 441W/m².

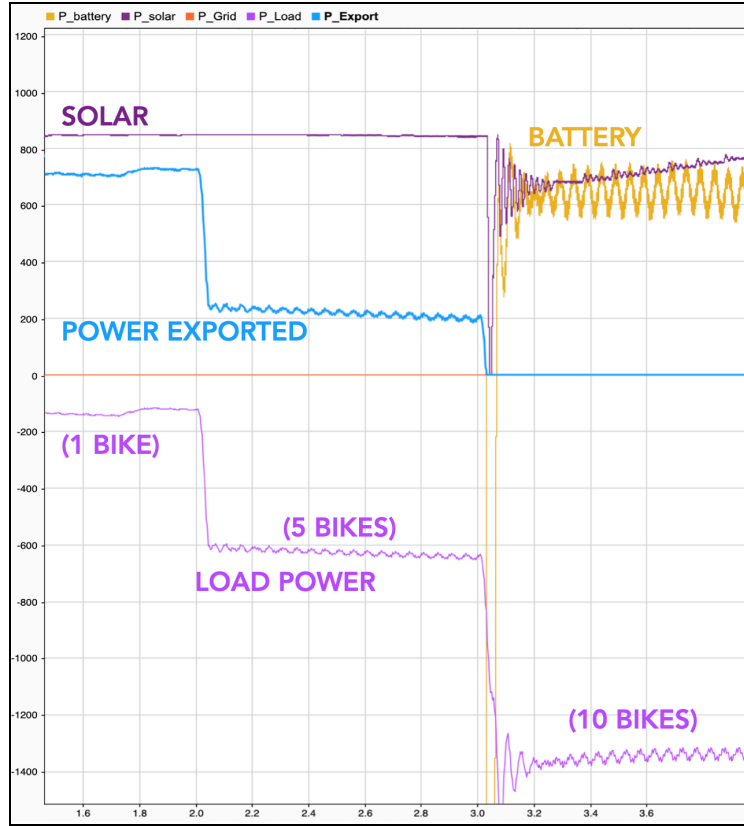


Figure 4.5.6 Simulation Power Results with Power Export mode

Analyzing this plot, we can see that the system is exporting power when the load of the system is 1 and 5 bikes, however, when 10 bikes are connected, the power exported is 0W because there is no surplus. Around 3.1seconds, we can see how the power from the battery transitions from 0W to 600W. This is because the power produced by the sun was not enough to meet the load demands, and the battery must aid in charging.

5 Conclusion

5.1 Improvements

5.1.1 Mechanical system

Whereas our prototype operated in a controlled environment, real-world outdoor deployment requires additional considerations especially when scaling up the system. Ensuring consumer security is our top priority, particularly regarding AC adapter safety. To address this concern, we can implement a mechanical locking mechanism that can be secured around the adapter, preventing theft.

We'll need to install a circuit breaker disconnect switch accessible from the outside of the enclosure to safely cut power when required. Raintight conduit fittings will enable flexible wiring

replacement as needed protecting the links between the solar array and enclosure. Adding a GFCI receptacle and junction boxes instead of the Type B outlet keeps users away from electrical boxes, mitigating risks from static discharge and other electrical hazards. Including clearly labeled wire terminals inside the enclosure allows for cleaner setups and safety to make maintenance easier. Using Galvanized steel poles provides longevity, resisting corrosion and damage better than PVC which is crucial for equipment meant to handle the elements. Finally, instead of using an above-earth grounding setup, ground rods driven directly into the earth establish a much more robust and reliable connection.

5.1.2 Charge controller

One improvement that could have been made to the charge controller is instead of hardwiring all of the configuration pins, jumper pins could have been used to more easily switch between different input supplies or output supplies. During testing, when connected to a DC power supply components needed to be removed, which is more difficult than using jumper pins. Additionally, a lot of the components chosen for the charge controller PCB were very small making design easy, but assembly very difficult. If designed again, nothing below an 0603 component would be included.

5.1.3 2-Stage Inverter

One improvement to the inverter stage would be to implement some form of digital feedback compensation based on measuring the output voltage. In this design, we relied on the stability of the boost converter to regulate the voltage at 170V. However, implementing some form of compensation on the inverter stage would more quickly respond to changes at the output, as well as allow for current control and regulation that can act as a protection method since it can shut down the circuit if the current exceeds a certain value; prior to the fuses blowing.

5.1.4 Software Ecosystem

In the current system, functionality has been implemented both to set the charge state to a specific port on the station, and to provide the capability to receive charge data from the initiated charging cycle. However, due to hardware time constraints, we were unable to fully explore and integrate this feature into the final project. Moving forward, we would like charging data to be accessible to the user along with adding a user login system using Flutter Firebase, which could track total usage within the system. This addition would enhance security, allow for personalized user interactions, and create the platform to add a payment system for a more production-ready product.

Furthermore, to enhance user experience, the introduction of more user notifications could be beneficial. For instance, implementing a notification system to alert users if the seven-segment display is currently in use for another user's Two-Factor Authentication (2FA) code could prevent conflicts and improve the overall reliability of the system. This conflict could also be resolved by expanding the system to incorporate more seven-segment displays, preparing for a larger pool of users. These enhancements,

collectively, would contribute to a more refined and versatile product with the potential for widespread adoption.

5.1.5 Simulation

Implementing the connection to the grid while the simulation was in export mode could be an improvement to the simulation. This would model the grid absorbing the power, and the net metering would be happening in real time, opposed to our approach which was to calculate the surplus power by comparing the power produced by the sun and the power demanded at the load. Another improvement would be to perform a simulation run through an entire day of 24 hours. This would cause the results to be a more accurate representation of battery behavior, load demands, and weather conditions.

5.2 Scaling and Next Steps

While our initial focus is on creating a prototype for the Northeastern campus, the impact of this project has the potential to extend well beyond campus boundaries. The success of our off-grid e-mobility charging station prototype and simulation modeling behavior in real-world, changing scenarios lays the foundation for adoption into other educational institutions, urban settings, and even corporate campuses. Future solutions of this project could include developing a grid-connected prototype with more charging slots to increase the usability and reliability of our system in communities where the number of e-mobility devices is ever increasing. This solution even has the potential to impact transportation in cities as a whole, as a network of multiple solar-power charging stations could play a transformative role in encouraging sustainability initiatives and urban transportation planning.

As next steps, our prototype will be refined based on user feedback and we will look for opportunities to optimize energy efficiency. Also, we will seek to build relationships with local authorities and utility companies, as future prototypes would have a higher chance of success in grid-connected and public space applications.



Figure 5.2: Grid Connected E-Mobility Charging Station

5.3 Closing Remarks

Our solar-powered e-mobility charging station project embodies our passion and dedication to sustainable engineering, innovative solutions, and effective collaboration. We believe that growing demand for e-mobility devices fused with cutting-edge technology and renewable energy principles has the power to reshape urban mobility and foster a wave of eco-friendly and safe transportation infrastructure. We look forward to witnessing the impact of our project in our immediate community, and hope to help pave the way for a greener and better connected future on campus and beyond. We would also like to express our gratitude to our advisor, Masoud Salehi, for his guidance and support throughout this endeavor.

6 Compliance

Below are a list of standards our team followed so our product was in compliance with regulatory requirements:

- IEEE 1547
- UL 1741 SA
- IPC-2221
- IPC-9592
- IEC 60269
- NEC 250
- NEC 314
- NEC 690
- NEC 310
- NEC 210

7 Acknowledgements

We acknowledge the following individuals who provided advice, insight, and guidance on various aspects of the project:

- Brad Lehman
- Herman Benson
- Pavel Dudek
- Edward Kelly
- Uthandi Selvarasu
- Shumeng Wang
- Anton Tinyakov

References

- [1] “The Micromobility Revolution: How Bikes And Scooters Are Shaking Up Urban Transport Worldwide,” CB Info. Services, Inc., New York, NY, Oct. 13, 2021.
- [2] “Micro-mobility Charging Infrastructure Market - Global Industry Analysis, Size, Share, Growth, Trends, Regional Outlook, and Forecast 2022 – 2030,” Precedence Res., Ottawa, ON, Rep. 1701, May 2022.
- [3] N. DuPuis, J. Griess, and C. Klein, “Micromobility in Cities. A History and Policy Overview,” Nat. League of Cities., Washington, DC, 2019.
- [4] “*2023 Guide to State & Local E-Bike Rebates & Tax Incentives*,” Juiced Bikes.
<https://www.juicedbikes.com/blogs/news/state-guide-electric-bike-rebates>
- [5] “*Electric Scooter Infrastructure: The Importance of Charging Stations and Parking Facilities*,” Gemopai. Jul. 24, 2023. <https://gemopai.com/electric-scooter-infrastructure-importance/>
- [6] “*How to Prevent Electric Scooter Battery Fires*,” Rider Guide. Jun. 16, 2022.
<https://riderguide.com/safety/how-to-prevent-electric-scooter-battery-fires/>
- [7] Linear Technology, “High Voltage, High Current Buck-Boost Battery Charge Controller with Maximum Power Point Tracking (MPPT),” LT8490 datasheet, 2014.
- [8] F. Hoffart, “*Proper Care Extends Li-Ion Battery Life*,” Electronic Design. Apr. 1, 2008.
<https://www.electronicdesign.com/markets/mobile/article/21190344/proper-care-extends-liion-battery-life>
- [9] Namboodiri, Anuja, and Harshal Wani. “*Unipolar and Bipolar PWM Inverter - IJIRST*”, International Journal for Innovative Research in Science & Technology, Dec. 2014,
www.ijirst.org/articles/IJIRSTV1I7111.pdf.
- [10] P. T. Krein, “Chp. 5.3 - 5.4.4,” in Elements of power electronics, New York: Oxford University Press, 2016
- [11] “*Using an IPC-2221 PCB Clearance Calculator for High Voltage Design*.” PCB Clearance for High Voltage Design, Altium, 27 Nov. 2023,
resources.altium.com/p/using-an-ipc-2221-calculator-for-high-voltage-design.

- [12] antz22. “*Antz22/Ultimate-Guide-to-Flutter: A Comprehensive Guide on Learning How to Code Cross Platform Mobile Applications with the Flutter Framework, from the Ground Up.*” GitHub, github.com/antz22/ultimate-guide-to-flutter. Accessed 12 Dec. 2023.
- [13] “*Simulink*,” MathWorks. <https://www.mathworks.com/help/simulink/>
- [14] “*Simscape Electrical*,” MathWorks. <https://www.mathworks.com/help/simulink/>
- [15] “*Climate Boston - Massachusetts*,” U.S. Climate Data. <https://www.usclimatedata.com/climate/boston/massachusetts/united-states/usma0046>
- [16] C. Cornwall, A. Horiuchi, and C. Lehman, “*Solar Position Calculator*,” NOAA Global Monitoring Laboratory. <https://gml.noaa.gov/grad/solcalc/azel.html>
- [17] “*Top 101 cities with the highest average wind speeds (population 50,000+)*,” City-data.com. <http://www.city-data.com/top2/c467.html>
- [18] NREL, “*NSRDB*”, nsrdb.nrel.gov/data-viewer.